Quantitative Phosphoproteomics Applied to the Yeast Pheromone Signaling Pathway*[S]

Albrecht Gruhler‡, Jesper V. Olsen‡, Shabaz Mohammed, Peter Mortensen, Nils J. Færgeman, Matthias Mann§, and Ole N. Jensen¶

Cellular processes such as proliferation, differentiation, and adaptation to environmental changes are regulated by protein phosphorylation. Development of sensitive and comprehensive analytical methods for determination of protein phosphorylation is therefore a necessity in the pursuit of a detailed molecular view of complex biological processes. We present a quantitative modification-specific proteomic approach that combines stable isotope labeling by amino acids in cell culture (SILAC) for quantitation with IMAC for phosphopeptide enrichment and three stages of mass spectrometry (MS/MS/MS) for identification. This integrated phosphoproteomic technology identified and quantified phosphorylation in key regulator and effector proteins of a prototypical G-protein-coupled receptor signaling pathway, the yeast pheromone response. SILAC encoding of yeast proteomes was achieved by incorporation of [$^{13}C_6$]arginine and [$^{13}C_6$]lysine in a double auxotroph yeast strain. Pheromone-treated yeast cells were mixed with SILAC-encoded cells as the control and lysed, and extracted proteins were digested with trypsin. Phosphopeptides were enriched by a combination of strong cation exchange chromatography and IMAC. Phosphopeptide fractions were analyzed by LC-MS using a linear ion trap-Fourier transform ion cyclotron resonance mass spectrometer. MS/MS and neutral loss-directed MS/MS/MS analysis allowed detection and sequencing of phosphopeptides with exceptional accuracy and specificity. Of more than 700 identified phosphopeptides, 139 were differentially regulated at least 2-fold in response to mating pheromone. Among these regulated proteins were components belonging to the mitogen-activated protein kinase signaling pathway and to downstream processes including transcriptional regulation, the establishment of polarized growth, and the regulation of the cell cycle. *Molecular & Cellular Proteomics 4: 310–327, 2005.*

Post-translational modifications are key regulators of protein function, activity, localization, and interactions. A major challenge in proteomics is to define the characteristics and dynamics of post-translational modifications in cells, tissues, and organisms (1, 2). Protein phosphorylation, one of the most important and best characterized post-translational modifications, plays a key role in eukaryotic signal transduction, gene regulation, and metabolic control in cells (3). Fundamental processes such as cell proliferation, adaptation, and differentiation are governed by reversible phosphorylation at specific serine, threonine, and tyrosine residues in proteins, and protein kinases and phosphatases are becoming major drug targets for a wide variety of diseases (4).

Phosphoproteomics of cell signaling events faces the challenge of low abundance proteins and low stoichiometry phosphorylation events. Thus, some of the most successful phosphoproteomic studies applied selective phosphoprotein and phosphopeptide enrichment techniques in combination with sensitive mass spectrometric peptide sequencing methods (2, 5). IMAC using either Ga(III) or Fe(III) as the ligand is highly useful for enrichment of phosphopeptides from complex mixtures and has enabled mass spectrometry-based phosphoprotein and phosphoproteome analysis in a variety of organisms, including yeast, plants, and humans (6–12). We have previously reported a phosphoproteomic technology that introduces peptide separation by strong anion exchange chromatography prior to affinity enrichment by Fe(III) IMAC and subsequent phosphopeptide separation and sequencing by nanoflow capillary LC-MS (7). Our conclusion from this study was that the performance of IMAC in large scale phosphoproteomics is critically dependent on peptide sample complexity and that subfractionation of complex peptide mixtures prior to IMAC is highly advantageous. In the present study we further explored this insight by combining strong cation exchange chromatography (SCX)[1] with IMAC and LC-MS in a quantitative phosphoproteomic study of the yeast pheromone response.

Another challenge in phosphorylation analysis by mass spectrometry is the fact that phosphorylation is generally a

[1] The abbreviations used are: SCX, strong cation exchange chromatography; SILAC, stable isotope labeling by amino acids in cell culture; LTQ, linear ion trap; GPCR, G-protein-coupled receptor; YNB, yeast nitrogen base; bis-Tris, 2-[bis(2-hydroxyethyl)amino]-2-(hydroxymethyl)propane-1,3-diol; SIM, selected ion monitoring; MAP, mitogen-activated protein; MEK, mitogen-activated protein kinase/extracellular signal-regulated kinase kinase; pS, phosphoserine; pT, phosphothreonine; pY, phosphotyrosine.

labile modification. In mass spectrometry-driven activated proteomics, protein identification is based on peptide fragmentation by collisionally activated tandem mass spectrometry (MS/MS) (13, 14) where cleavages of covalent bonds mainly occur through the lowest energy pathways (15). If the peptide involved contains a labile post-translational modification, this becomes the preferred site of fragmentation (energetically favored cleavage) because the energy needed to dissociate the post-translational modification bond is much lower than that of a peptide amide bond. Depending on how facile the post-translational modification cleavage is, it can severely hamper efficient backbone fragmentation by MS/MS and thereby peptide identification. This is particularly the case for phosphoserine- and phosphothreonine-containing peptides, and the effect is often more pronounced in ion trap type analyzers than in quadrupole TOF type analyzers.

To overcome this inherent challenge of phosphopeptide sequencing, a number of different MS fragmentation techniques have been applied. Electron capture dissociation and the related electron transfer dissociation have been reported to successfully sequence phosphopeptides with preservation of the phosphate moiety on most fragment ions (16–18). Both methods are based on the capture of a thermal electron by a multiply protonated peptide leading to charge state reduction with subsequent c and z type peptide backbone fragmentation.

Another powerful approach to the identification of labile phosphopeptides is to introduce additional stages of tandem MS. In ion traps, the abundant neutral loss product ions can be further isolated, fragmented, and analyzed, a process termed MS/MS/MS (MS^3). This strategy has been successfully used in a recent large scale phosphoproteomic experiment using a three-dimensional ion trap with software-controlled neutral loss-dependent MS^3 capabilities (19). More than 2000 phosphorylation sites from HeLa cells were identified on the basis of MS^3.

We have previously developed online LC-MS^3 for large scale peptide identification (20) using a hybrid linear ion trap (LTQ)-FT mass spectrometer (21). Accurate parent ion masses combined with the information contained in MS^3 spectra led to several orders of magnitude higher certainty of peptide identification. We now applied this LC-MS^3 approach to phosphoproteomic analysis by specifically sequencing phosphorylated peptides by two consecutive stages of tandem mass spectrometry. We used the neutral loss-dependent MS^3 mode of operation where the diagnostic loss of phosphoric acid (-98 Da) from the precursor ion detected in a MS/MS scan automatically triggered data-dependent MS^3 fragmentation of the neutral loss precursor ion. Previous large scale phosphoproteomics studies have provided a tremendous amount of data that can be interrogated by bioinformatic sequence analysis for novel insights into protein kinase recognition sites, phosphorylated protein domain structure, protein-protein interactions, and cellular signaling events (22).

However, from a biological point of view, regulated phosphorylation, such as phosphorylation induced by a cell stimulus, is of particular interest. To investigate regulated phosphorylation, quantitative proteomics has to be used; this has been done only in a very few cases (23, 24). Recently, Moran and co-workers (25) have used methylation with normal or deuterated methanol to determine changes in the epidermal growth factor-induced phosphoproteomes of human tumor cells in the presence or absence of a chemical inhibitor. We and (later) another group have described stable isotope labeling by amino acids in cell culture (SILAC) as a generic quantitative proteomic technology (26–28) and applied SILAC to determine signal-induced multiprotein complexes, protein-protein interactions, and the time order of activation of signaling pathways (29–31). In the present study, we combined SILAC with phosphoproteomics to examine and quantify changes in protein phosphorylation in the yeast pheromone signaling pathway.

G-protein-coupled receptor (GPCR) signaling is one of the best characterized molecular mechanisms by which chemical and sensory signals are transduced from cell surface receptors to intracellular effector molecules. GPCRs encompass the largest family of cell surface receptors in eukaryotes and are of immense interest in pharmacology and biotechnology research. The yeast *Saccharomyces cerevisiae* is widely used as a model system for studies of GPCR-mediated signaling and has provided many key insights into mitogen-activated protein kinase pathways, including the pheromone response involved in mating of yeast cells (32–34). Here we report the quantitative study of pheromone-induced phosphorylation changes by a combination of phosphoproteomic technologies. We have identified a large number of phosphorylation sites that are pheromone-regulated and discuss their biological significance in the pathway. This is the largest yeast phosphoproteomic study and demonstrates the requirements and feasibility of studying the regulation of signaling pathways.

EXPERIMENTAL PROCEDURES

Materials—Yeast nitrogen base (YNB) without amino acids and terrific broth were purchased from BD Biosciences. Agar, yeast extract, and bacto-peptone were from Remel (Lenexa, KS). Tyrosine was from MP Biochemicals (Irvine, CA), adenine was from Sigma, and all other amino acids were from SERVA Electrophoresis GmbH (Heidelberg, Germany). [$^{13}C_6$]Arginine and [$^{13}C_6$]lysine were bought from Cambridge Isotope Laboratories, Inc. (Andover, MA).

Generation of Yeast Strain YAL6B—*S. cerevisiae* strains Y00981 (BY4741; *MAT*a; *his3Δ1*; *leu2Δ0*; *met15Δ0*; *ura3Δ0*; *YHR018c::kanMX4*) and Y15969 (BY4742; *MATα*; *his3Δ1*; *leu2Δ0*; *lys2Δ0*; *ura3Δ0*; *YIR034c::kanMX4*) were purchased from EuroScarf and crossed to generate YAL6B. Standard methods were used for the generation of zygotes, sporulation, tetrad analysis, and selection of strains with a double deletion of *arg4* and *lys1* genes. Briefly, Y00981 and Y15969 were grown separately on YPD (1% yeast extract, 2% bacto-peptone, 2% glucose, 2% agar, 200 mg/liter adenine) culture dishes for 24 h at 30 °C. Zygotes were generated by mixing equal amounts of both strains on a YPD plate and incubating them for 8 h at 30 °C. Cells

were replica-plated, and diploid cells were selected on YNB drop-out medium lacking lysine and arginine (6.7 g/liter yeast nitrogen base without amino acids, 2% glucose, 2% agar, 200 mg/liter adenine, 200 mg/liter tyrosine, 10 mg/liter histidine, 60 mg/liter leucine, 10 mg/liter methionine, 60 mg/liter phenylalanine, 40 mg/liter tryptophane, 20 mg/liter uracil). For sporulation, diploid cells were grown YNB plates, transferred to GNA (5% D-glucose, 3% terrific broth, 1% yeast extract, 2% agar) presporulation plates and grown for 1 day at 30 °C. Cells were repatched on a fresh GNA plate and incubated for another day at 30 °C. A small amount of cells was transferred to 2 ml of sporulation medium (1% potassium acetate, 0.005% zinc acetate, 60 mg/liter leucine, 20 mg/liter uracil, 10 mg/liter histidine) and incubated for 5 days at 25 °C followed by 3 days at 30 °C.

Cells were washed with sterile water and resuspended in 50 μl of 50 mg/ml zymolyase T100 (Seikagaku Kogyo, Tokyo, Japan) in 1 M sorbitol and incubated for approximately 10 min at 30 °C. Digestion of asci was followed by examining aliquots under a microscope, and the reaction was stopped by placing the samples on ice and adding 150 μl of sterile H_2O. A small amount of cells was transferred to a strip of YPD agar on a sterile microscope slide for tetrad analysis. Spores were dissected, separated with a glass needle, and grown on YPD medium for 3 days at 30 °C. Cells were then transferred to YNB plates and selected for Arg⁻/Lys⁻ double auxotrophs.

To determine the mating type, cells were grown in liquid YPD medium at 30 °C until they reached early logarithmic phase. α-Factor (2 μM) was added, and cells were examined by phase-contrast microscopy for the formation of mating tips. One colony with mating type *MATa*, termed YAL6B, was chosen for further experiments. It was not determined whether YAL6B carried the *met15Δ0* and *lys2Δ0* mutations.

Labeling of Yeast Cells with Stable Isotopes and Treatment with α-Factor—Two cultures of 100 ml of liquid YNB medium containing either 100 mg/liter arginine and lysine or 100 mg/liter [$^{13}C_6$]arginine and [$^{13}C_6$]lysine were inoculated with a small amount of YAL6B cells from a stationary YPD culture (dilution ~1:6000). Yeasts were grown by rotation at 180 rpm for 16 h at 30 °C until they reached an A_{600} between 0.6 and 0.7. α-Factor (2 μM) was added to the unlabeled culture, and cells were incubated for an additional 2 h at 30 °C, at which point they had reached an A_{600} of ~1.4. Equal amounts of cells from both cultures (as determined by A_{600} measurement) were added to a flask containing ice and mixed. Cells were harvested by centrifugation for 5 min at 3000 × g at 4 °C, resuspended in cold H_2O, and centrifuged once more, and the cell pellet was frozen at −80 °C. Cells corresponding to 100 ml of the mixed culture were used for further isolation of phosphopeptides (as described below).

Preparation of Yeast Protein Extracts for Analysis by Gel Electrophoresis—Yeast cells corresponding to 1 A_{600} unit were harvested by centrifugation and resuspended in 1 ml of cold H_2O. Cells were disrupted by alkaline lysis, and proteins were isolated by precipitation with TCA. Briefly, 150 μl of lysis buffer (1.85 M NaOH, 7.5% (v/v) 2-mercaptoethanol) were added, and the samples were vortexed. After a 10-min incubation on ice, the suspensions received 150 μl of 50% TCA solution, were vortexed briefly, and were kept on ice for a further 10 min. Precipitated proteins were pelleted by centrifugation for 10 min at 20,000 × g at 4 °C. The pellets were resuspended in 100 μl of sample buffer (5% SDS, 8 M urea, 200 mM Tris/HCl, 1.5% (w/v) DTT, 0.1 mM EDTA, 0.03% bromphenol blue) by shaking the samples at 37 °C. Proteins were separated by one-dimensional SDS-PAGE.

Gel electrophoresis was performed with NuPage® bis-Tris gels and buffer (Invitrogen) according to the instructions of the manufacturer. The gels were stained with Coomassie using SimplyBlue™ SafeStain (Invitrogen). Protein bands were excised and digested with trypsin. The gel bands were cut into small cubes of ~1 mm³ that were washed twice with 50 μl of H_2O followed by 50 μl of 50% acetonitrile

for 10 min each on a mixer. Supernatants were discarded after each washing step. The gel pieces were dehydrated by the addition of 50 μl of acetonitrile. Disulfide bonds were cleaved by incubating the samples for 30 min at 37 °C with 50 μl of 2 mM DTT in 100 mM ammonium bicarbonate buffer. Alkylation of cysteines was performed by the addition of 50 μl of 10 mM iodoacetamide in 100 mM ammonium bicarbonate buffer and incubation of the samples for 30 min at room temperature in darkness. Gel bands were washed once with H_2O and 50% acetonitrile and dehydrated with 50 μl of acetonitrile. Gel pieces were covered with trypsin solution (12.5 ng/μl in 50 mM ammonium bicarbonate buffer). After a 45-min incubation of ice, the remaining trypsin solution was removed, and 25 μl of 50 mM ammonium bicarbonate were added. Proteolysis was performed overnight at 37 °C and stopped by adjusting the samples to 5% formic acid. The supernatant was directly used for analysis by mass spectrometry.

Isolation of Phosphopeptides from Yeast Cells—Frozen yeast cells were resuspended in 1 ml of lysis buffer (137.93 mM NaCl, 8.06 mM Na_2HPO_4, 2.67 mM KCl, 1.47 mM KH_2PO_4, 0.5% n-octylglucoside, 1 mM sodium orthovanadate, 2.5× phosphatase inhibitor mixture 1 (Sigma)), and ~750 μl of acid-washed glass beads were added. The cells were disrupted by vortexing for 5 × 1 min with 1-min intervals where the samples were cooled on ice. The sample mixture was centrifuged for 8 min at 5000 × g at 4 °C, and the supernatant was transferred to a new tube. The pellet was washed with 0.5 ml of lysis buffer also containing 0.2% RapiGest (Waters Corp., Milford, MA) and centrifuged again. This supernatant was combined with the previous one and precleared by centrifugation for 15 min at 20,000 × g at 4 °C. The supernatant was transferred to a new tube, and its protein concentration was determined to be 4.6 μg/μl by Bradford analysis (Bio-Rad) using bovine serum albumin as standard.

Protein extract corresponding to 2.8 mg of protein was brought to 8 M urea by the addition of urea. Proteins were reduced by the addition of 5 mM DTT and incubation for 30 min at 50 °C. The sample was cooled to room temperature prior to the addition of 20 mM iodoacetamide. Alkylation of cysteines was performed by incubating the samples for 30 min at room temperature in darkness. 5 μg of endoproteinase Lys-C (Calbiochem-Novabiochem) were added to the protein extract followed by incubation for 3 h at 37 °C. To facilitate proteolysis with trypsin, the sample was diluted 4-fold with 100 mM NH_4HCO_3. 20 μg of trypsin (Promega Corp., Madison, WI) were added, and proteolysis continued for 16 h at 37 °C. To inactivate Lys-C and trypsin and to cleave the RapiGest detergent, 25 mM HCl was added to the sample, which was then kept for 2 h at 37 °C.

Desalting of the sample was performed with an Oasis HLB plus cartridge (Waters Corp.). Peptides were eluted with 90% acetonitrile, 0.5% formic acid and dried to near completion *in vacuo* followed by acidification with formic acid. The peptide solution was brought to 30% acetonitrile, 2.5% formic acid and centrifuged for 8 min at 20,000 × g at 4 °C.

Strong cation exchange chromatography was performed on a 1-ml Resource S column (Amersham Biosciences) on an Ettan instrument (Amersham Biosciences). The precleared peptide mixture was loaded onto a 100-μl injection loop and separated with a linear gradient from 100% buffer A (30% acetonitrile, 5 mM ammonium formate, pH 2.7) to 60% buffer B (30% acetonitrile, 1 M ammonium formate, pH 3.0) at a flow rate of 0.6 ml/min. Fractions corresponding to 0.6 ml (fractions 1–4) and 0.3 ml were collected and frozen at −70 °C until further analysis.

Phosphopeptides were enriched by IMAC from the first 14 SCX fractions. The sample volume of SCX fractions was reduced *in vacuo* to 20–40 μl. 150 μl of W/B buffer (30% acetonitrile, 0.25 mM acetic acid) and 30 μl of equilibrated IMAC beads (Phos-Select, Sigma) were added. The samples were rotated in Mobicol spin columns with 10-nm plugs (MoBiTec, Goettingen, Germany) for 2 h at room tem-

perature. IMAC beads were washed twice with 200 μl of W/B buffer and once with 200 μl of H_2O, and peptides were eluted by incubating the IMAC beads twice with 50 μl of elution buffer (50 μM KH_2PO_4/ NH_3, pH 10.0) for 5 min. The eluates were acidified with 5 μl of acetic acid and frozen at -70 °C. Prior to analysis by mass spectrometry, the samples were desalted with C_{18} STAGE tips (35).

LC-MS/MS and MS³ Analysis—Nanoscale liquid chromatography tandem mass spectrometry (nano-HPLC-MS/MS) experiments were performed on an Agilent 1100 nanoflow system (Agilent Technologies) connected to a 7-tesla Finnigan LTQ-FT mass spectrometer (Thermo Electron, Bremen, Germany) equipped with a nanoelectrospray ion source (Proxeon Biosystems, Odense, Denmark) as described previously (36) with a few modifications.

Briefly the mass spectrometer was operated in the data-dependent mode to automatically switch between MS, MS/MS, and neutral loss-dependent MS³ acquisition. Survey full scan MS spectra (from m/z 300 to 1575) were acquired by FTICR with resolution $r = 25,000$ at m/z 400 (after accumulation to a target value of 5,000,000 in the linear ion trap). The three most intense ions were sequentially isolated for accurate mass measurements by a FTICR "selected ion monitoring (SIM) scan," which consisted of a 15-Da mass range, $r = 50,000$, and a target accumulation value of 80,000. These were then simultaneously fragmented in the linear ion trap using collision-induced dissociation at a target value of 10,000.

The data-dependent neutral loss algorithm in the Xcalibur software was enabled for each MS/MS spectra. Data-dependent settings were chosen to trigger a MS³ scan when a neutral loss of 98, 49, or 32.7 Da was detected among the 10 most intense fragment ions.

Former target ions selected for MS/MS were dynamically excluded for 30 s. Total cycle time was approximately 3 s. The general mass spectrometric conditions were: spray voltage, 2.4 kV; no sheath and auxiliary gas flow; ion transfer tube temperature, 100 °C; collision gas pressure, 1.3 millitorrs; normalized collision energy using wide band activation mode; 35% for both MS² and MS³. Ion selection thresholds were: 250 counts for MS² and 10 counts for MS³. An activation q = 0.25 and activation time of 30 ms was applied in both MS² and MS³ acquisitions. Initial LC-MS/MS analyses of incorporation of labeled amino acids was performed on an LC Packings system (Ultimate; Switchos2; Famos; LC Packings, Amsterdam, The Netherlands) coupled to a Q-TOF Micromass spectrometer (Micromass UK Ltd., Manchester, UK) as described previously (37).

Data Base Searches: Peptide Identification—All MS/MS spectra files from each LC run were centroided and merged to a single file, which was searched using the MASCOT search engine (Matrix Science) against the publicly available yeast_orf data base (*Saccharomyces* Genome Database, Stanford University) with carbamidomethyl cysteine as fixed modification. Protein *N*-acetylation, oxidized methionine, phosphorylation (serine, threonine, and tyrosine), and $[^{13}C_6]$lysine and $[^{13}C_6]$arginine were searched as variable modifications. Searches were done with tryptic specificity allowing two missed cleavages and an initial tolerance on mass measurement of 5 ppm in MS mode and 0.5 Da for MS/MS ions.

To determine the appropriate precursor mass accuracy suited for high mass accuracy peptide data base searching in this experiment, we performed an initial search with a conservative parent mass accuracy of 10 ppm. From this search we calculated the average ($\mu = 0.17$ ppm) as root mean square and standard deviation ($\sigma = 1.45$ ppm) on parent mass errors of the 300 highest scoring peptides. Because all the mass errors follow a normal distribution, we can make sure at least 99.9% of the measured parent ion population is within the parent mass accuracy by specifying an initial parent mass accuracy $\geq \mu \pm 3.29 \cdot \sigma = 4.94$ ppm (99.9% confidence interval). We therefore decided to use 5 ppm.

Peptide Validation and Quantification—All identified phosphopep-

tides were manually validated, and localization of phosphorylated residues within the individual peptide sequences were manually assigned using the in-house written software MSQuant, which is an open source software (msquant.sourceforge.net/) that handles LTQ-FT raw files. Relative quantification ratios of the identified phosphopeptides were derived by MSQuant as previously described (38). Briefly peptide ratios between the monoisotopic peaks of "normal" and "heavy" forms of the phosphopeptide were calculated and averaged over consecutive MS cycles for the duration of their respective LC-MS peaks in the total ion chromatogram using both FT survey and FT SIM scans.

RESULTS AND DISCUSSION

Generation of Yeast Strains and SILAC Labeling with $[^{13}C_6]$Arginine and $[^{13}C_6]$Lysine—Cellular protein expression levels and regulation of protein activity mediated by post-translational modifications vary greatly in response to developmental or environmental changes, and quantitation of protein expression is therefore an important aspect of proteomic studies. In this study, stable isotopes were incorporated into yeast proteins by labeling the cells with SILAC to quantify alterations of protein phosphorylation in response to mating pheromone. The combination of modified amino acids used for SILAC and the sequence specificity of the protease used determines which peptides are modified after proteolytic cleavage of proteins. With a combination of $[^{13}C_6]$arginine and $[^{13}C_6]$lysine, maximal labeling of tryptic peptides is achieved, and the loss of quantitative data for a portion of the identified peptides is avoided (23). Wild type *S. cerevisiae* can synthesize all amino acids, which might lead to incomplete incorporation of modified amino acids during *in vivo* labeling of cells. To circumvent this potential problem, we generated the yeast strain YAL6B that is auxotrophic for arginine and lysine by crossing two strains with deletions of either *lys1* or *arg4* genes, producing a diploid strain that is heterozygous for both genes. Sporulation and dissection of asci enabled the selection of haploid strains with disruptions of both *lys1* and *arg4* genes.

To test the incorporation of modified arginine and lysine, YAL6B cells were grown either in the presence of $[^{13}C_6]$arginine and $[^{13}C_6]$lysine or in unmodified medium for 16 h (approximately 10 generations). Proteins were extracted from both samples and separated by one-dimensional gel electrophoresis. Gel bands corresponding to the same proteins were excised from the two samples, digested with trypsin, and analyzed by nanoflow LC-tandem MS. A typical example of lysine- and arginine-containing peptides is shown from enolase 2 (Fig. 1). Masses of both peptides (AVD-DFLLSLDGTANK, 789.91 m/z) and (SGETEDTFIADLVVGLR, 911.52 m/z) increased by 6 Da in their isotope-labeled forms corresponding to the incorporation of one $[^{13}C_6]$arginine or $[^{13}C_6]$lysine. No unmodified peptides were detected in the isotope-encoded samples, demonstrating that incorporation of $[^{13}C_6]$arginine or $[^{13}C_6]$lysine was close to completion. The labeled peptides exhibited a skewed isotope distribution and a minor peak with a mass difference of -1 Da (Fig. 1, marked
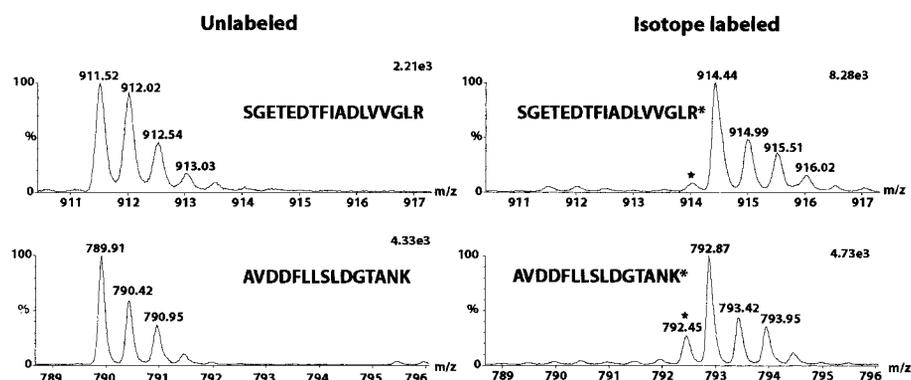
FIG. 1. **Efficient incorporation of [$^{13}C_6$]arginine and [$^{13}C_6$]lysine in yeast proteins.** YAL6B yeast cells were grown in the presence of [$^{13}C_6$]arginine and [$^{13}C_6$]lysine or unmodified medium. Proteins were extracted from both samples, separated by gel electrophoresis, and analyzed by in-gel digestion and LC-MS/MS on a Q-Tof instrument. Mass spectra of arginine- and lysine-containing tryptic peptides from enolase 2 are shown in their unmodified (*left panels*) and isotope-labeled forms (*right panels*).

with an *asterisk*). This is due to a small percentage of ^{12}C atoms in the ^{13}C-marked amino acids used in our experiments. As observed previously, a proportion of [$^{13}C_6$]arginine was converted to [$^{13}C_5$]proline leading to a reduction in the intensity of the isotope-labeled peptide peak (27). This was corrected for during the quantitation of proline-containing peptides with MSQuant. Analysis and quantification of several other randomly chosen proteins confirmed the excellent labeling efficiency (not shown). All of the identified proteins became efficiently marked with $^{13}C_6$, making YAL6B a suitable strain for double labeling with [$^{13}C_6$]arginine or [$^{13}C_6$]lysine in SILAC experiments.

Phosphopeptide Enrichment Strategy—The aim of this study was the quantitative analysis of phosphorylation changes in yeast in response to the mating pheromone α-factor. To accomplish this, several known proteomic techniques had to be improved and combined. Fig. 2 depicts an outline of the experimental approach taken.

YAL6B *MAT* **a** yeast cells were cultured for approximately 10 generations in the presence of [$^{13}C_6$]arginine and [$^{13}C_6$]lysine until they reached early logarithmic phase. α-Factor was added to the unlabeled cells, and both cultures were incubated for an additional 2 h. YAL6B cells responded to the addition of α-factor with the formation of pear-shaped mating projections ("shmoos") and a large decrease in the number of budding cells (not shown). These morphological changes are hallmarks of the pheromone response and require activation of the MAP kinase signaling cascade through α-factor. Equal amounts of α-factor-treated and control cells were mixed and harvested. Cells were disrupted by vortexing them with glass beads in a buffer containing phosphatase inhibitors and *n*-octylglucoside, a detergent compatible with subsequent analysis of samples by mass spectrometry. Proteins were denatured with urea and proteolyzed with a combination of endoprotease Lys-C and trypsin. The resulting peptide mixture was desalted on a reverse phase cartridge and loaded onto a SCX column. Peptides were separated using an am-

monium formate gradient instead of the more commonly used sodium chloride gradient because this volatile salt allowed further processing of samples without a desalting step that often leads to loss of peptides. SCX, performed at pH 2.7, has been used before for the enrichment of phosphopeptides (19). Due to their low pK_a value, phosphate groups are partially protonated at pH 2.7, in contrast to carboxyl and amine groups. Therefore, phosphopeptides have a lower charge than the majority of tryptic peptides and elute in the first fractions during SCX. In addition to phosphopeptides, we observed accumulation of two other classes of peptides in the first SCX fractions: *N*-acetylated peptides and carboxyl-terminal peptides, which both are reduced in charge compared with internal unmodified tryptic peptides (not shown). A small amount of the early SCX fractions was analyzed by LC-MS/MS to examine the proportion of phosphopeptides in these fractions. As the vast majority of identified peptides was nonphosphorylated, we chose to further enrich phosphopeptides with IMAC. The first 14 of 35 fractions of an SCX gradient were subjected to batch purification of phosphopeptides using commercially available Fe(III)-loaded IMAC beads. This additional affinity purification increased the proportion of phosphopeptides up to 50% in some fractions (not shown), which in turn improved the success rate of phosphopeptide sequencing by tandem mass spectrometry.

Analysis of Phosphopeptides by MS—Tandem mass spectra of serine/threonine phosphopeptides are often less informative because the majority of precursor ions readily undergo elimination of phosphoric acid. This can result in a prominent neutral loss ion (MH$_n^{n+}$ − H_3PO_4) particularly in ion trap type mass spectrometers where it often constitutes the most abundant fragment ion. This hinders sequence annotation, and in many cases the assignment of phosphopeptides and phosphorylation sites is not possible.

To identify phosphopeptides, data base search programs typically generate all possible phosphorylated variants of each tryptic peptide in the data base. There are many com-
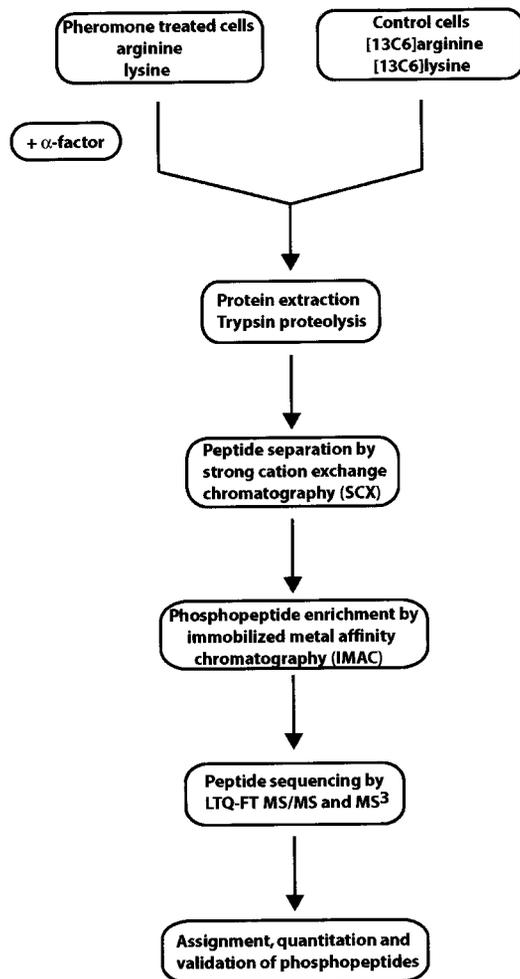
FIG. 2. **Schematic overview of experimental approach.** Shown is the enrichment and mass spectrometric analysis strategy of phosphopeptides from SILAC labeled, pheromone-treated yeast YAL6B cells. For further details see text.

binatorial possibilities of placing zero or one phosphate group on each serine, threonine, and tyrosine; this leads to a large increase in the number of theoretical spectra that need to be compared with each fragmentation spectrum. Combined with the fact that phosphopeptide spectra are often of less information content than the spectra of unmodified peptides and the fact that phosphoproteins are often only identified by a single peptide, it is frequently difficult to ascertain whether a phosphopeptide has been correctly identified. This problem is further exacerbated by modern mass spectrometers and proteomic strategies that can obtain tens of thousands of fragment spectra in a single project. Together, these factors may lead to either uncertainty in the obtained phosphorylation assignments or to a large percentage of phosphopeptides that have been sequenced but that cannot be assigned easily.

To assure correct identification of phosphopeptides in this project, we made use of three factors: (i) accurate precursor ion mass, (ii) two consecutive stages of fragmentation (MS^3),

and (iii) the presence of all phosphopeptides in SILAC pairs (except carboxyl-terminal peptides). Our approach relies on the high mass accuracy and fast MS^3 capabilities of a LTQ-FT mass spectrometer in combination with on-line nanoflow LC separation. The LTQ-FT is a dual mass spectrometer with two independent detection systems (FTICR and LTQ), which can be operated simultaneously. After obtaining a survey spectrum, narrow mass range spectra (SIM scans) are recorded for all precursors that are selected for sequencing. In the SIM scan mode, after iterative recalibration (39), we obtained an average absolute mass accuracy of 0.6 ppm in this experiment (see Supplemental Table 1). Compared with typical mass accuracies obtained with an ion trap alone, the accurate parent ion mass increases search specificity by more than a factor of 100.

When serine/threonine-phosphorylated peptides are fragmented under collision-induced dissociation MS/MS conditions, the main fragmentation pathway is gas-phase elimination of phosphoric acid with the subsequent conversion of phosphoserine and phosphothreonine to dehydroalanine and 2-aminodehydrobutyric acid, respectively. Gygi and co-workers (19) have used MS^3 to further fragment these dephosphorylated species in a three-dimensional ion trap. MS^3 events were triggered whenever loss of phosphoric acid was detected. Here we use the LTQ-FT, which has the advantage that precursor ions can be measured exceedingly accurately, many more precursor ions can be stored, the scans are faster, and hence the MS^3 spectra are both richer in information and much faster to acquire. In particular, the large dynamic range of the LTQ allows observation of low level, but significant, ions in the MS^3 spectra.

Fig. 3*A* shows an overview of the scan cycle used. Peptide precursors are analyzed by SIM in the FTICR and are fragmented simultaneously in the LTQ by MS^2 as well as by neutral loss-driven MS^3. Fig. 3*A* illustrates the scan cycle scheme with a sequence set-up to perform one FT survey full scan followed by three FT SIM, three LTQ MS/MS, and up to three neutral loss-dependent MS^3 in less than 3 s. Since the phosphopeptides occur in heavy and light isotope pairs, up to four different fragment spectra (2× MS/MS and 2× MS^3) are acquired for each phosphopeptides. Fig. 3*B* shows the identification of a phosphorylation site of the pheromone receptor Ste2p via four fragmentation spectra. Although these MS^3 spectra are redundant in case of a correct identification (as shown in the figures) in case of misidentification they would be completely different and would not provide fragment ions related to the supposed peptide sequence. The fact that they are derived from the neutral loss precursor ion confirms the peptide assignment and the fact that it is a phosphopeptide.

We have previously shown that searching a peptide with both the MS/MS and MS^3 fragmentation spectra leads to very high confidence in identification (20). To utilize the information in both spectral types, we searched MS/MS spectra with the MASCOT search engine, specifying possible serine, threo-
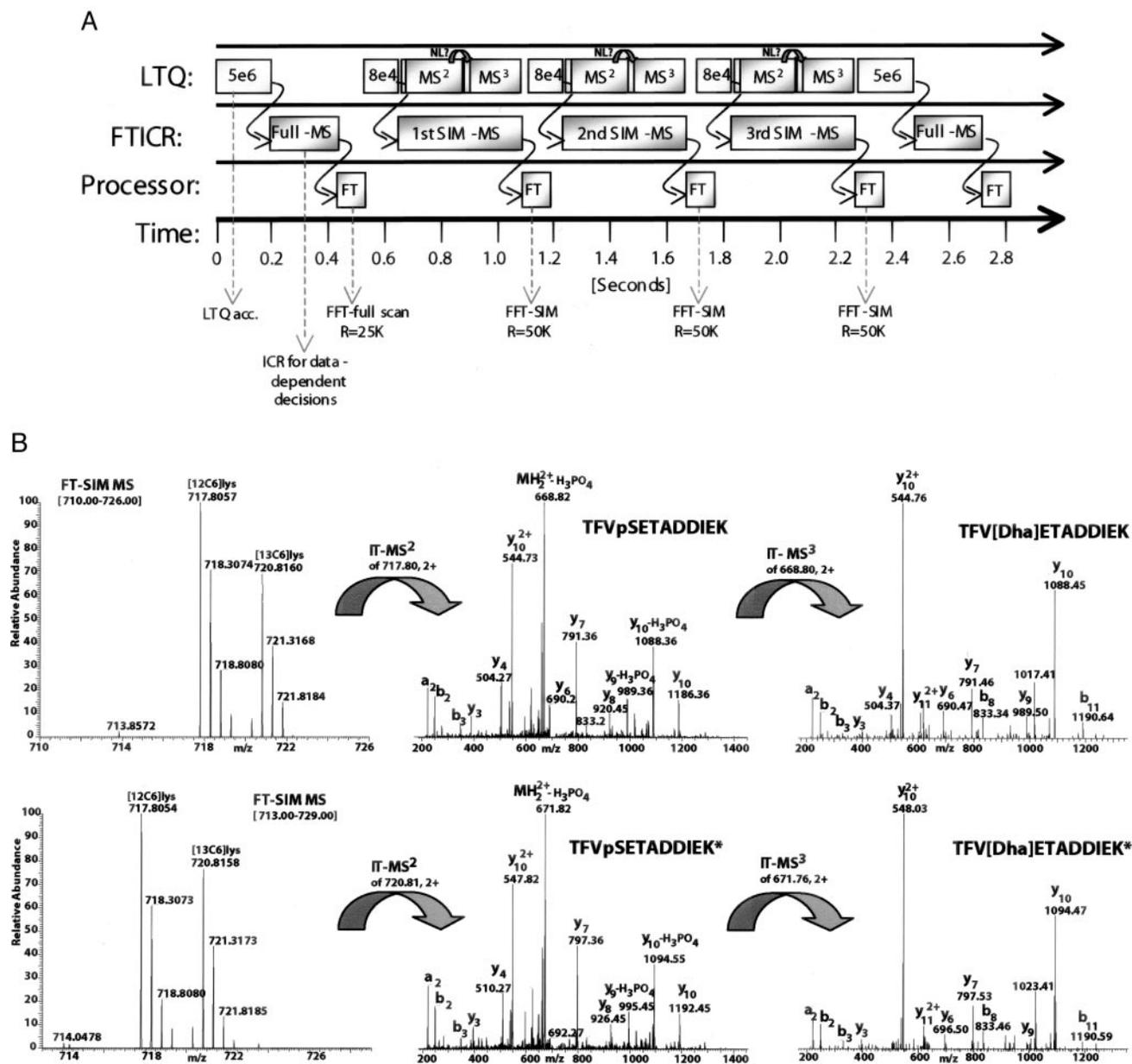
FIG. 3. *A*, LTQ-FT neutral loss-dependent MS[3] scan cycle. Scan times and set-up for phosphopeptide-specific MS[3] identification are shown. The LTQ-FT mass spectrometer has two independent detection systems (LTQ and FTICR), which can be operated simultaneously. For data-dependent decisions, a MS[1] full scan is acquired in the FTICR cell for a high dynamic range survey of the total mass range. The three most abundant ions are, in turn, isolated and analyzed. To achieve sub-ppm mass accuracy we acquired a SIM scan in the FTICR of the each peptide ion, which at the same time in the LTQ is fragmented and analyzed (MS[2]). If a neutral loss precursor ion is detected among the 10 most intense fragment peaks during the MS[2] event, a MS[3] spectrum is automatically generated of this ion. *B*, overview of SILAC phosphopeptide pair identification and quantitation by LTQ-FT analysis. Each phosphopeptide is sequenced and consequently identified by up to four independent MS[n] fragmentation events. Identification of the phosphopeptide TFVpSETADDIEK from Ste2p (α-factor pheromone receptor) is based on FT-SIM, ion trap (*IT*)-MS[2], and ion trap-MS[3] of both the heavy and the light SILAC encoded peptide. The *top panel* shows the consecutive MS events for the light isotope version of the phosphopeptide. The *top left* spectrum displays the SIM FTICR-MS[1] experiment of the precursor ion to obtain sub-ppm mass accuracy. The *top middle spectrum* shows the MS[2] of the same peptide ion that is isolated and fragmented in the linear ion trap to obtain sequence information. The *top right spectrum* displays the phosphospecific MS[3]; the neutral loss precursor ion derived from MS[2] is isolated and fragmented further. The *lower panel* displays the same for the heavy isotopic form of this phosphopeptide. *NL*, neutral loss; *acc.*, accumulation; *FFT*, fast Fourier transformation; *Dha*, dehydroalanine.

nine, and tyrosine phosphorylation. MS[3] spectra were also assigned the parent mass of the phosphorylated species in the SIM scan and searched in MASCOT specifying possible

dehydroalanine and 2-aminodehydrobutyric acid instead of serine and threonine. In this way, each phosphopeptide could be identified in up to four independent searches. Importantly

FIG. 4. **Differentially regulated phosphorylation sites within a protein.** Two phosphopeptides from the Cdc28p serine/threonine protein kinase were identified with different ratios. The *upper panel* shows the identification of the threonine-phosphorylated sequence AYpTHEIVTL-WYR by MS[2] and MS[3] (*middle* and *right panels*). From the FTICR-SIM scan (*upper left panel*) the relative ratio between the heavy and light isotopic forms is calculated to be close to 1:1, hence there was no significant change in this phosphorylation site upon α-factor stimulus. The *lower panel* shows identification of the tyrosine-phosphorylated peptide VGEGTpYGVVYK by SIM and MS[2]. The [$^{13}C_6$]lysine-labeled form (control cell population) of the peptide precursor ion is more than 5 times more abundant than the normal labeled version (α-factor-treated). *IT*, ion trap; *MeDha*, 2-aminodehydrobutyric acid.

even low scoring spectra, when combined with higher scoring spectra of a SILAC partner or another fragmentation stage, are highly significant. Only phosphopeptides for whom a SILAC partner was detected were accepted. While it is possible that "on-off" phosphorylation changes would be missed by using these criteria, this is unlikely as our dynamic range was sufficiently high that none of the arginine- or lysine-containing phosphopeptides with significant identification score appeared as singletons.

While most phosphopeptides lose the phosphate group as the major fragmentation pathway, a significant percentage is relatively stable (40). These include almost all phosphotyrosine-containing peptides but also many serine/threonine-phosphorylated peptides. Importantly these peptides tend to have informative MS/MS spectra and were identified in this way in our experiment. As an example, see the peptide from Cdc28p cyclin-dependent kinase in Fig. 4 that is phosphorylated on tyrosine residue 19. The resulting MS/MS spectrum does not contain any abundant fragment peaks corresponding to the neutral loss of phosphoric acid.

In total, we recorded 54,045 MS/MS fragmentation events and neutral loss-triggered acquisition of 8984 MS[3] spectra. The MS[3] spectra led to the identification and assignment of 3438 phosphopeptides in the yeast proteome. Each phosphopeptide was typically sequenced and identified in several

forms (SILAC pairs, oxidized methionine, and different charge states). After eliminating this redundancy, 729 unique phosphorylation sites were determined in 503 different proteins. On the basis of the high parent mass accuracy and the fact that in our strategy several fragmentation spectra identify the same site, we believe that these phosphopeptides assignments are of very high confidence. In contrast, only 417 unique phosphopeptide sequences could be identified in MASCOT by MS/MS alone (~57%) with a score higher than 24 (95% confidence threshold).

While phosphopeptide identification became essentially automated, we found that assignment of phosphorylation sites in these peptides was not always achieved unambiguously by the search engine. Instead we used raw MS/MS and MS[3] spectra in the MSQuant software to distinguish between various possible phosphorylation patterns, for example in serine-rich peptides. Electron capture dissociation or electron transfer dissociation may be able to eliminate this remaining problem in phosphopeptide identification in the future since all fragment ions tend to retain their modifications.

Analysis of Phosphopeptides—This study comprises the largest data set of yeast phosphoproteins to date. 724 phosphopeptides and 729 individual phosphorylation sites originating from 503 proteins were identified by mass spectrometry, quantified for relative expression levels in response to

TABLE I
List of identified differentially regulated phosphopeptides

The presented ratios and standard deviations are calculated by averaging intensity-weighted SILAC ratios from consecutive FT-MS scans during the elution of the individual peptide pairs. H/L ratio, heavy to light isotope ratio.

Name	Phosphopeptide sequence	H/L ratio	S.D.	Reciprocal ratio
NRP1	AQEILpSPFPQSK	0.07	0.01	14.1
SEC16	TpSPSPTGPNPNNSPSPSSPISR	0.07	0.01	14
AFR1	pSNSTSNLFALSSTFSK	0.07	0.03	14.2
FUS3	IIDESAADNSEPTGQQSGMTEpYVATR	0.09	0.01	10.7
FAR1	TGQLSALQpSPVNITSSNK	0.12	0.05	8.1
FUS3	IIDESAADNSEPTGQQSGMpTEYVATR	0.12	0.01	8.6
MKT1	SNLSpSPSSASSSASPATTVTK	0.13	0.01	7.8
NOP4	VLSIpTPTLVR	0.13	0.02	7.7
INP52	LLpSPTKEISIVSVSPR	0.14	0.02	6.9
DIG2	NLQQLGMLLVpSPGLDEDRLSEK	0.15	0.03	6.6
PUF4	QTFHALpSPTDLINAANNVTLSK	0.16	0.06	6.4
SEC10	LTNVTQVVpSPLGDKLETAIK	0.16	0.01	6.2
SST2	NLpSNENCSFK	0.16	0.04	6.1
IPP1	GIDLTNVTLPDpTPTYSK	0.17	0.03	5.9
RPC53	EIQEALSEKPTREPpTPSVK	0.18	0.07	5.5
SST2	NLpSNENCpSFKK	0.18	0.02	5.4
YDR261C-D	AHNVSTSNNpSPSTDNDSISK	0.18	0.01	5.4
CHD1	GPAALINNTRLSPNSPpTPPLK	0.19	0.03	5.2
PIK1	SSpTPTSPIDLIDPIK	0.21	0.04	4.8
STE2	NQFYQLPpTPTSSK	0.21	0.01	4.7
DCS1	LNLIWPApTPIHIK	0.22	0.01	4.6
PIK1	SSTPTpSPIDLIDPIK	0.22	0.04	4.6
RRP5	GGASALpTPLELK	0.22	0.02	4.6
STE12	LVpSPSDPTSYMK	0.22	0.07	4.6
YDR261C-D	NVLpSK	0.22	0.07	4.6
TAF4	NVpSPTTNLR	0.24	0.08	4.2
FUN30	VASSSPLKPTpSPTVPDASVASLR	0.24	0.03	4.1
SAS4	NNAASIpSPTLSEK	0.25	0.12	4
YDR261C-D	pSPSIDASPPENNSSHNIVPIK	0.25	0.03	4
FUN30	VASSpSPLKPTSPTVPDASVASLR	0.25	0.03	4.0
DIG1	TSQPQQQpSPSLLQGEIR	0.26	0.03	3.8
VPS27	LTLSNpSPTAMFDSK	0.26	0.04	3.9
STE20	TFNTTTGLPGpSPQVSTPPANSFNK	0.27	0.08	3.8
PSK1	GDYGNNIpSPERPSFR	0.28	0.04	3.6
YDR034C-C	MESQQLSQNpSPNLHGSAYASVTSK	0.28	0.11	3.5
MRH1	APVApSPRPAATPNLSK	0.29	0.05	3.4
SSE2/SSE1	GAAFICAIHpSPTLR	0.29	0.03	3.4
SST2	APNGpSTIDLDFTLR	0.29	0.04	3.4
TFP1	GIDpTPALDR	0.29	0.1	3.4
YDR034C-C	VNNDHINESTVSSQYLpSDDNELSLRPATERI	0.29	0.08	3.4
MRH1	APVApSPRPAApTPNLSKDK	0.3	0.04	3.4
LSP1	ALLELLDDSPVpTPGEARPAYDGYEASR	0.30	0.04	3.4
TFC7	TAGLLpSPTEENETTNAGQSK	0.31	0.09	3.2
WHI5	NGFGTPSPPpSPPGITK	0.32	0.03	3.1
YBR025C	VIVPpSPR	0.32	0.04	3.1
YDR261C-D	TVPQIpSDQETEKR	0.34	0.04	3
CDC19	NCpTPKPTSTTETVAASAVAAVFEQK	0.35	0.07	2.9
SEC16	TNSAISQpSPVNYAFPNPYK	0.36	0.03	2.8
RPL13A	APEAEQVLpSAAATFPIAQPATDVEAR	0.38	0.09	2.6
SOD1	FEQASESEPTTVSYEIAGNpSPNAER	0.38	0.08	2.6
STB4	LIpSFQMGR	0.38	0.06	2.6
SHE3	TNVTHNNDPSTpSPTISVPPGVTR	0.39	0.09	2.6
SIS1	SASSpSPTYPEEETVQVNLPVSLEDLFVGKK	0.39	0.11	2.6
SSB2	VTPSFVAFpTPQER	0.39	0.01	2.6
YDR098C-B	MESQQLSNYPHIpSHGSACASVTSK	0.39	0.04	2.5
NIS1	SNTpSPSVLYHPK	0.4	0.11	2.5
PPQ1	AGSFGAPSpSPTSGIPNPK	0.4	0.05	2.5
YOR192C-A	MESQQLSQNpSPTFHGSAYASVTSK	0.4	0.09	2.5

TABLE I—*continued*

Name	Phosphopeptide sequence	H/L ratio	S.D.	Reciprocal ratio
DPS1	AYLAQpSPQFNK	0.41	0.04	2.4
NUP159	SLpSPTSEKIPIAGQEQEEK	0.41	0.1	2.4
VPS27	ANSpSPTTNIDHLK	0.41	0.04	2.4
YDR261C-D	SPpSIDASPPENNSSHNIVPIK	0.41	0.03	2.4
AHP1	pSDLVNKK	0.41	0.00	2.5
MDS3	ISApSSLPIPIENFAK	0.42	0.02	2.4
SMY2	APIGTVVpSPYSK	0.42	0.01	2.4
VIP1	NNLPSAPSEMpSPLFLNK	0.43	0.02	2.4
WSC2	FSATpSLPDMMEER	0.43	0.14	2.3
GFD1	IpSPVSESLAINPFSQK	0.43	0.05	2.3
HXT3	MNSTPDLISPQK	0.43	0.00	2.3
FAS2	VVEIGPpSPTLAGMAQR	0.44	0.06	2.3
CDC15	SAIPSSSSLPLSSpSPTR	0.45	0.1	2.2
CYR1	EATpTPTIETPISCKPSLFR	0.45	0.06	2.2
HXT1	MNSpTPDLISPQK	0.45	0.11	2.2
CUE2	GIHSIGGIpSKVR	0.46	0.05	2.2
PFK26	RYpSVIPTAPPSAR	0.46	0.06	2.2
RPG1	TAGGSpSPATPATPATPATPTPSSGPK	0.46	0.01	2.2
STP3	SIpSPILK	0.46	0.03	2.2
YOR220W	GGSSLpSPDKSSLEpSPTMLK	0.46	0.01	2.2
ZRG8	TPIIGNENLTSTTpSPSNLEPAIR	0.46	0.11	2.2
ZEO1	LEETKEpSLQNK	0.47	0.1	2.1
RLR1	VIPPApSPSQASILTEEVIR	0.48	0.03	2.1
IPP1	AASDAIPPApSPKADAPIDK	0.48	0.08	2.1
LSB3	FTAPTpSPSTSSPK	0.48	0.02	2.1
CRP1	pSPALPQADDPIVETK	0.49	0.11	2.1
FAR11	SVpSLEDLKR	0.49	0.1	2
MSN4	RGpSTIpSPTTTINNSNPNFK	0.49	0.04	2
SEC16	ESIIpSTGSEFLPPPK	0.49	0.12	2.1
ADR1	FSpTPELVPLDLK	0.50	0.05	2.0
GRS1	YDIGNPVTGETLEpSPR	0.50	0.05	2.0
YRA1	SANLDKpSLDEIIGSNK	8.8	2.65	0.1
DBF2	LVGFpTFR	6.22	1.95	0.2
RFA2	GYGpSQVAQQFEIGGYVK	5.76	0.91	0.2
GIN4	NFpSLQTRPVSR	5.55	2.07	0.2
CDC28	VGEGTpYGVVYK	5.03	1.24	0.2
ESC1	NLpSDLENYSQR	4.82	0.88	0.2
SWI4	ILENpSPILYR	4.79	0.28	0.2
SWI5	FVISETPpSPVLK	4.72	0.74	0.2
BOI2	SApSEAIKGETLK	4.40	0.71	0.2
COG3	TKpSSSILTLAR	4.02	0.01	0.2
SHS1	FLNpSPDLPER	3.95	0.25	0.3
SHS1	NIpSETVPYVLR	3.81	0.17	0.3
MCM3	LQLGLRVpSPR	3.73	0.87	0.3
BUD4	LSSpSPLKFTLK	3.63	0.62	0.3
NUP60	SNVVVAETpSPEKK	3.56	0.52	0.3
BEM3	ALGFpSPASK	3.53	0.40	0.3
MAD3	QLpTPILEMR	3.49	0.93	0.3
YBR255W	IATpTPEAQISR	3.44	0.53	0.3
GIN4	LSTIVNQSpSPTPASR	3.41	0.01	0.3
ORC6	NQLFGpTPTK	3.28	0.85	0.3
YOL070C	LLSpSPLRQEK	3.22	0.37	0.3
STB1	SQPQMpSPEKEQELASK	3.21	0.01	0.3
SHO1	NTpTPYQNNVYNDAIR	3.11	0.01	0.3
MSC3	RLpSTSSAAPPTSR	2.94	1.44	0.3
RPL12B	IGPLGLpSPK	2.84	0.24	0.4
BFR1	KVVADDLVLVpTPK	2.79	0.19	0.4
ELC1	pSQDFVTLVSKDDKEYEISR	2.78	0.01	0.4
MMR1	NAGSFQNLLNpSPTK	2.59	0.55	0.4
YMR031C	KIpSGYGNDLDAQK	2.57	0.73	0.4
SPA2	NYWDVNDpSPIIKVDK	2.48	0.23	0.4

TABLE I—*continued*

Name	Phosphopeptide sequence	H/L ratio	S.D.	Reciprocal ratio
TSL1	pSATRpSPSAFNR	2.46	0.48	0.4
CDC11	pSGIIDASSALRK	2.4	0.36	0.4
ACE2	GLpSGTAIFGFLGHNK	2.37	0.36	0.4
TSL1	IApSPIQQQQQDPTTNLLK	2.35	0.22	0.4
HBT1	pSISGGTFGFR	2.34	0.05	0.4
GGA1	VSLSpSPKSPQENDTVVDILGDAHSK	2.28	0.55	0.4
RNR1	EApSPAPTGSHSLTK	2.27	0.28	0.4
BUD3	LGDDYpSDKETAK	2.19	1.64	0.5
NET1	SFLPPPTQPQpSPPIR	2.18	0.16	0.5
ESC1	SNIFSpSPIR	2.15	0.28	0.5
CDC3	QLELSINSApSPNVNHSPVPTK	2.09	0.32	0.5
GFA1	EVGApSMTR	2.06	0.08	0.5

α-factor, and manually validated (for complete list see the supplemental information). Only a small portion of these phosphorylation sites has been identified in a previous global analysis of phosphopeptides in yeast (9) or is annotated in the Swiss-Prot data base. Ficarro and colleagues (9) enriched *O*-methyl esterified phosphopeptides with IMAC from total yeast cell lysate and found mostly multiphosphorylated peptides.

Using a combination of SCX and IMAC without additional derivatization of peptides in our experimental set-up, we mainly recorded singly phosphorylated peptides, which might explain the small overlap. Interestingly, all the doubly phosphorylated peptides observed in our data set contained one missed cleavage and therefore had two basic lysine or arginine amino acids in their sequence. This increase in peptide basicity could help to maintain the same charge state as singly phosphorylated peptides containing one basic residue by balancing the charge shift caused by the second acidic phosphate group. Therefore, similar elution behavior from SCX and IMAC columns could be expected of both classes of peptides. The fact that we mainly identified singly phosphorylated peptides using the SCX/IMAC combination is consistent with our previous study where strong anion exchange chromatography/IMAC was used (7). Thus, either strong anion exchange chromatography or SCX can be used to reduce the sample complexity prior to IMAC enrichment of phosphopeptides in large scale phosphoproteomics.

The phosphorylated proteins in our data set where almost all named gene products rather than anonymous open reading frames and therefore likely represent the abundant phosphorylation sites in yeast. They fall into many different functional categories, including protein, RNA, lipid and carbohydrate metabolism, organelle biogenesis, morphogenesis, and vesicle-mediated transport. In addition, proteins from different cellular locations and organelles were found, including nuclear proteins and membrane proteins. Our experimental approach is therefore suited to study the regulation of a wide variety of cellular processes taking place in different subcellular locations.

Regulated Phosphorylation in Pheromone-treated Cells— Since proteins involved in signal transduction generally are of low abundance and phosphorylation can be substoichiometric, it was not known at the onset of this study whether and how many phosphoproteins that participate in pheromone signaling could be detected. Quantitation of the MS data revealed, however, that 139 phosphopeptides changed in concentration by at least a factor of 2: 89 phosphopeptides were pheromone-induced, and 42 peptides were down-regulated (Table I). Taken together, 18% of the detected phosphopeptides were regulated by α-factor, demonstrating that it is feasible to study the effects of mitogen activation on the phosphoproteome of yeast by this approach.

Changes in the amounts of phosphopeptides can be due to either pheromone-induced phosphorylation and dephosphorylation, changes in protein synthesis and degradation rates, or a combination of both. For example, phosphorylation of factor arrest protein Far1p by Fus3p is induced by α-factor, and in addition its expression is up-regulated about 5-fold by Ste12p (41). Therefore, the observed 8-fold induction is most likely the result of increased phosphorylation and transcription. Alterations in the phosphorylation of some cell cycle-regulated proteins might be a consequence of the changes in their respective expression levels due to the growth arrest of pheromone-treated cells in G_1 phase. However, in a number of cases, several phosphopeptides with distinct phosphorylation sites were identified that belonged to the same protein. In some of these instances, the amounts of all phosphopeptides shifted similarly or remained constant, whereas in other cases changes differed for specific phosphopeptides. For the latter class of proteins, changes in the amount of phosphopeptides are most likely due to regulated phosphorylation and not to changes in protein abundance levels. One example is the cyclin-dependent kinase Cdc28p, of which two phosphopeptides [14]VGEGTpYGVVYK[24] and [167]AYpTHEIVTL-WYR[178] were detected (Fig. 4). Phosphorylation at tyrosine 19 has been implicated in the inhibition of Cdc28p kinase activity, whereas phosphorylation at threonine 169 activated the enzyme (42). We observed pheromone-induced down-regu-
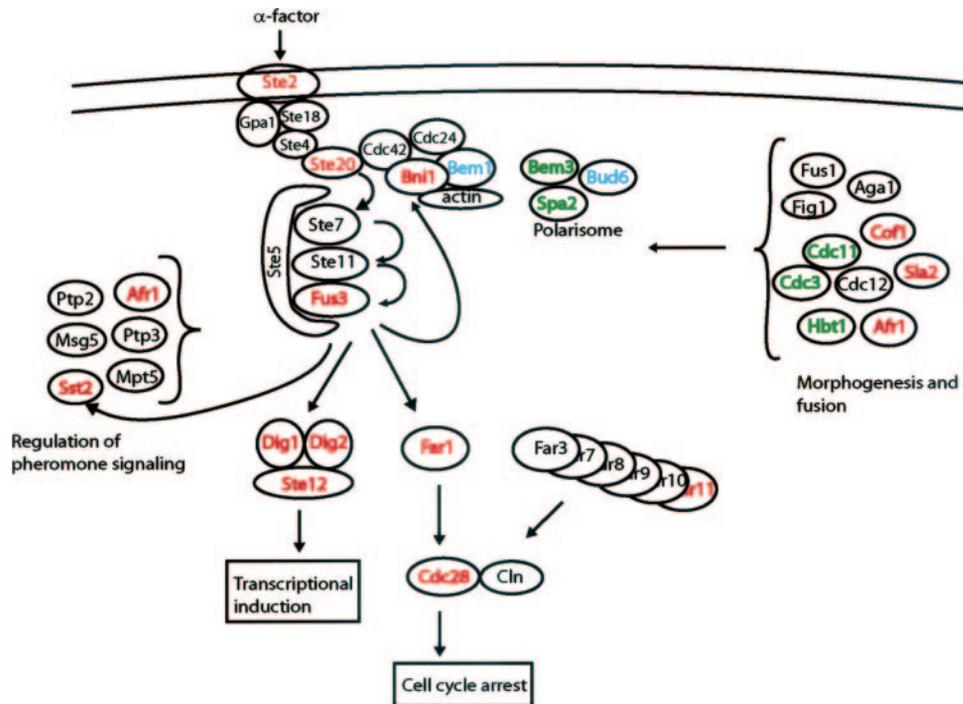
FIG. 5. **Schematic overview of pheromone signaling pathway highlighting identified regulated phosphoproteins.** Binding of α-factor to its receptor Ste2p triggers the activation of a MAP kinase cascade, which is mediated by the trimeric G-protein (consisting of Gpa1p, Ste4p, and Ste18p) and Cdc42p. Activation of the MAP kinase Fus3p occurs via successive phosphorylation of the p21-activated kinase Ste20p, MEK kinase Ste7p, and MEK Ste11p. Substrate phosphorylation by Fus3p is required for pheromone-induced transcriptional regulation, cell cycle arrest, morphologic changes, and feedback regulation of signaling. Known targets are the transcription factors Ste12p, Dig1p, and Dig2p; the factor arrest protein Far1p; the G-protein regulator Sst2p; and the actin-interacting protein Bni1p. The other factors shown in this figure contribute to different aspects of conjugation and are described in greater detail under "Results." Increased phosphorylation was found for proteins marked in *red*, decreased phosphorylation was found for proteins marked in *green*, unchanged (<1.5-fold) phosphorylation was found for proteins in marked in *blue*, and no phosphopeptides were detected for proteins marked in *black*.

lation of phosphotyrosine 19 by a factor of 5 in contrast to the unchanged threonine 169 phosphorylation. This suggests that inhibition of Cdc28p activity by Far1p during pheromone-induced cell cycle arrest does not require the inhibitory phosphorylation of Cdc28p on tyrosine 19 but is achieved by a different mechanism.

Phosphorylation Events in the Pheromone Pathway—Pheromone signaling in yeast is well characterized, and years of research have revealed many of the factors and mechanisms responsible for the pheromone-induced cellular processes. Signal transduction in the yeast pheromone pathway is a complex multistep process involving both G-protein signaling and protein phosphorylation by mitogen-activated kinases (33) (Fig. 5). The receptor for α-factor is Ste2p, a member of the GPCR family that is associated with a trimeric G-protein consisting of Gpa1p (Gα), Ste4p (Gβ), and Ste18p (Gγ). Binding of α-factor induces the dissociation of Gpa1p from the Ste4p/Ste18p subunits. Released G$\beta\gamma$, in concert with the Rho-type GTPase Cdc42p, binds and thereby induces the p21-activated kinase Ste20p (43, 44). Active Ste20p triggers the successive phosphorylation of the MEK kinase Ste11p, the MEK Ste7p, and the MAP kinase Fus3p. These three

kinases are assembled into a complex by the scaffold protein Ste5p that also interacts with Gβ thereby recruiting all players of the pheromone-dependent signaling cascade in close proximity to the initial site of signaling (45). Up-regulated phosphopeptides were identified for Ste2p, Ste20p, and Fus3p (Fig. 5), demonstrating the ability of our proteomic approach to capture activation of key components of the yeast pheromone signaling cascade.

Substrate phosphorylation by the MAP kinase Fus3p is essential for downstream processes in pheromone signaling such as transcriptional regulation, cell cycle arrest, morphogenesis, and adaptation to pheromone signaling. In this study, a large number of regulated phosphopeptides have been found from proteins that are known to mediate different aspects of pheromone-induced cellular changes (Fig. 5). Phosphorylation of three transcription factors, Ste12p, Dig1p, and Dig2p, was strongly increased upon incubation of cells with α-factor (Table I). Ste12p, which is phosphorylated by Fus3p, is essential for the transcriptional activation of many genes participating in signal transduction, morphogenesis, feedback regulation of the pathway, and cellular fusion (41, 46). Transcriptional activation by Ste12p is inhibited by Dig1p and

TABLE II
Functional classification for a subset of differentially regulated phosphopeptides

Functional category	Increased phosphorylation	Reduced phosphorylation
Pheromone signaling and regulation	Ste2p, Ste20p, Fus3p, Afr1p, Sst2p	
Pheromone-induced transcription	Dig1p, Dig2p, Ste12p	
Pheromone-induced cell cycle arrest	Far1p Far11p	
Regulation of actin cytoskeleton	Inp52p, Smy2p, Lsb3p, Vip1p	Cog3p, Bem3p, Spa2p
Vesicular transport	Sec16p Vps27p, Sec10p	Gga1p
Cell cycle-regulated genes	Cyr1p, Nis1p, Whi5p, Dbf2p, Cdc15p	Ace2p, Mcm3p, Net1p, Rfa2p, Stb1p, Swi4p, Dbf2, Cdc28p, Swi5p Mad3p, Orc6p, Msc3p,
Cell budding and cytokinesis	Pik1p	Bud3p, Bud4p, Cdc11p, Gin4p, Shs1p, Cdc3p, Mmr1p
RNA transcription, processing, transport, and metabolism	Rrp5p, Stp3p, Gfd1p, Nop4p, Puf4p, Dcs1p, Nup159p, Rlr1p, Taf4p, Rpc53p, Tfc7p	Yra1p
tRNA, translation and ribosomal	Dps1p, Grs1p, Stp3p, Rpg1p, Rpl13Ap	Elc1p, Tif3p
Heat shock proteins and stress response	Ssb2p, Sse1p, Msn4p, Sod1p, Sis1p, Ahp1p, Zrg8p	
Meiosis	Mds3p, Pds1p	Gfa1p

Dig2p, two associated transcriptional repressors, and phosphorylation of these two factors by Fus3p is thought to release active Ste12p (47, 48).

Up-regulated phosphopeptides were identified from Far1p (8-fold) and Far11p (2-fold), two proteins involved in pheromone-induced cell cycle arrest in G$_1$ phase. Genetic data indicate that Far1p, which is subject to phosphorylation by Fus3p (46), is essential for the cell cycle arrest initiation, whereas Far11p in concert with other factors might be required for its continuation (49, 50). Far1p interacts with Cdc28p-G1 cyclin complexes, and it has been proposed that it exerts its function through inhibition of the Cdc28p-Cln kinase activity (51–53), although the significance of this finding has been debated (54). Phosphorylation of Far1p on serine 87 and threonine 306 is important for Far1p stability and its association with Cdc28p-Cln2p, respectively (54). We identified a peptide with a phosphorylation site on serine 114 with unknown biological role.

Pheromone-induced morphogenesis is a complex process that comprises the establishment of cellular polarization, the reorganization of the actin cytoskeleton, endocytosis of the Ste2p receptor, directed vesicular transport, the formation of mating projections, and finally cell fusion. Genetic and biochemical evidence suggest that a landmark for polarization is established in proximity to the initial signaling site by the interaction of components of the signaling cascade, *e.g.* Ste2p, G$\beta\gamma$, Ste20p, and Cdc42p-Cdc24p, with proteins participating in actin regulation and formation of the mating projection (55–57). We have detected novel phosphorylation sites for a number of proteins known to take part in cellular polarization and mating tip formation (Fig. 5), indicating that pheromone-induced morphogenesis is tightly regulated by phosphorylation. An example for this class of proteins is Bni1p, a known Fus3p substrate that interacts with Cdc42p and actin

(58). A phosphopeptide of Bni1p was detected that was induced 2-fold by α-factor. Other examples for proteins with pheromone up-regulated phosphorylation include Sla2p, a protein involved in the polarization of cortical actin and endocytosis (59); the actin-binding protein Cof1p; Ede1p that is involved in the endocytosis of Ste2p; and Vps27p, found to be required for the transport of internalized Ste2p to vacuoles (60).

Mating projections become restricted at their base at high concentrations of α-factor, similar to the buds of dividing yeast cells (61). A subset of proteins that localize to the bud necks has also been detected in mating projections, such as the septins Cdc3p, Cdc11p, and Cdc12p, chitin synthase Chs3p, the polarisome subunits Bud6p and Spa2p, and the Cdc42 regulator Bem3p. We identified regulated phosphopeptides of Cdc3p, Cdc11p, Spa2p, Bem3p, and Bud6p (Table I). Interestingly their phosphorylation was reduced or remained constant (Bud6p) in the presence of pheromone, indicating that their regulation during cell conjugation differs from the budding process of vegetatively growing cells.

Proteins, such as Fus1p, Fus2p, Fig 1p, Aga1p, and Prm1p, known to participate directly in cellular fusion were absent from our data set, although their expression is up-regulated on the transcriptional level by pheromone (41, 57). One could therefore speculate that if these proteins become phosphorylated, this might occur at a later phase of conjugation, which might require contact with cells of the opposite mating type and is not reached by incubation of cells with α-factor only.

Cells treated with mating pheromone for prolonged time without successful cell fusion finally recover from cell cycle arrest and recommence vegetative growth. Adaptation to pheromone signaling is achieved by the modulation of the sensitivity and concentration of the Ste2p receptor, G-protein signaling, and kinase activity. We found induced phosphoryl-
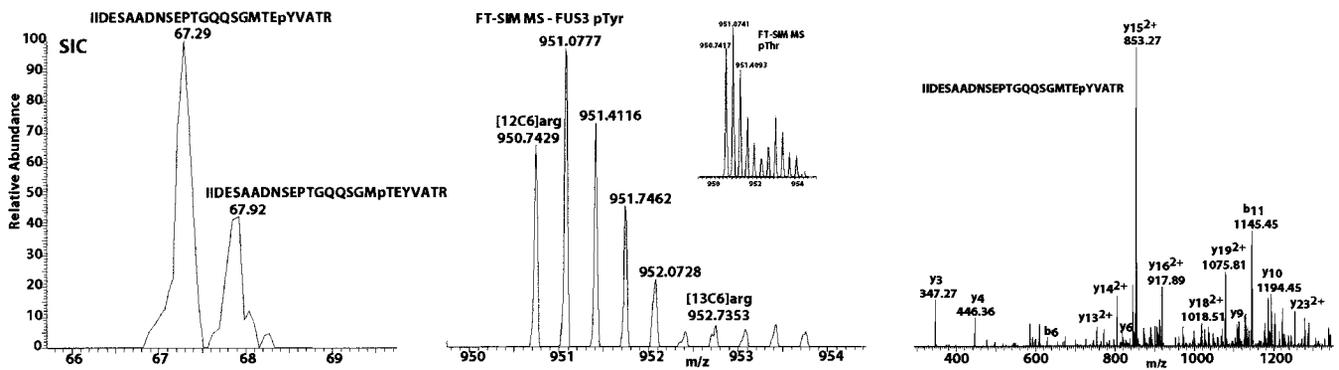
FIG. 6. **Isobaric phosphopeptide detection.** The Fus3p phosphopeptide sequence IIDESAADNSEPTGQQSGMTEYVATR was identified in both a threonine- and a tyrosine-phosphorylated version. The *left panel* shows the extracted ion chromatogram as a function of retention time for this phosphopeptide. Clearly two discrete isobaric peptides elute within 1 min of each other. The *middle panel* displays the FTICR SIM scan for the early eluting peptide pair (phosphotyrosine (*pTyr*) peptide) where the *inset* shows the SIM scan for the late pair (phosphothreonine (*pThr*) peptide). The *right panel* displays the MS^2 of the heavy isotope peak from the early eluting phosphopeptide, which identifies the tyrosine-phosphorylated version of the peptide.

ation for Sst2p and Afr1p, known to be involved in feedback regulation of pheromone signaling. Sst2p, a known substrate of Fus3p, increases the GTPase activity of Gpa1p, thereby shortening the half-life of active GTP-bound Gpa1p (62–64).

Besides the proteins with known relation to pheromone signaling and morphogenesis, we detected regulated phosphoproteins falling into different functional categories (subset shown in Table II). Phosphorylation of cell cycle-regulated proteins was generally decreased, which is in good agreement with their transcriptional repression by pheromone (41). Induced phosphorylation was observed, however, for Cdc15p, Dbf2p, and Nis1p, which are regulators of mitosis. Dbf2p phosphorylation is dependent on Cdc15p and promotes exit from mitosis (65). If α-factor is added to a yeast culture, *MAT* **a** cells that have initiated the cell cycle will finish mitosis before they arrest in G$_1$ phase. Increased amounts of Cdc15p and Dbf2p phosphorylation may reflect the larger number of cells in late stages of mitosis. In addition, increased phosphorylation was observed for Whi5p, a transcriptional repressor of the heteromeric SBF transcription factor that promotes transition from G$_1$ to S phase (66). Interestingly Whi5p is hyperphosphorylated by Cdc28p-Cln during G$_1$ phase, leading to its dissociation from SBF. Since pheromone-induced arrest in G$_1$ phase leads to a decrease in Cdc28p activity, it can be speculated that the observed induction of Whi5p phosphorylation is caused by another kinase and might positively regulate Whi5p activity.

α-Factor induced the phosphorylation of several proteins involved in RNA processing and transport (Table II). An interesting example is She3p that has been found to interact with mRNA, myosin Myo4p, and She2p (67). These proteins are required for the polarized transport of Ash1 mRNA along actin cables to the bud. A role for She3p in transport of mRNAs in mating cells has not been shown yet, but one could speculate that during conjugation specific mRNAs are also transported to the mating projection.

In conclusion, the regulated phosphopeptides in our data set reflect pheromone-induced phosphorylation, thereby demonstrating for the first time that quantitative phosphoproteomics is a suitable tool for the characterization of signaling pathways. A large number of phosphopeptides were identified from known members of the pheromone signaling pathway, covering all aspects of yeast conjugation, including the α-factor receptor, kinases of the MAP kinase pathway, transcription factors, and effector proteins involved in regulation of signaling, polarization, and mating tip formation.

Analysis of Phosphorylation Sites—A detailed characterization of all the phosphorylation sites that were identified in this study is beyond the scope of this publication. We will therefore limit our analysis to the immediate members of the pheromone signaling pathway and to known targets of Fus3p. Pheromone-induced phosphopeptides were identified from the following members of the pheromone signaling cascade: Ste2p, Ste20p, and Fus3p (Table I), but there were no phosphopeptides found from Ste5p, Ste11p, and Ste7p. A recent large scale analysis examined the expression levels of epitope-tagged yeast proteins expressed from their natural promoters (68). Copy numbers per cell for proteins of the pheromone signaling cascade ranged from 260 (Ste20p) to 1900 (Ste5p). Neither Ste5p, Ste7p, Ste11p, nor Ste20p are transcriptionally induced by α-factor. However, the number of phosphorylated species could be quite different from the total protein number, and this may account for the lack of detected phosphopeptides from Ste5p, Ste11p, and Ste7p. On the other hand, we identified phosphorylated Ste20p, which is a low copy number protein, demonstrating the sensitivity of our approach.

Specific phosphorylation sites have been reported for Fus3p. Activation of the pheromone signaling cascade leads to its phosphorylation at threonine 180 and tyrosine 182 by the dual specificity MEK Ste11p, and mutation of either residue abolishes kinase activity (69). In this study, two Fus3
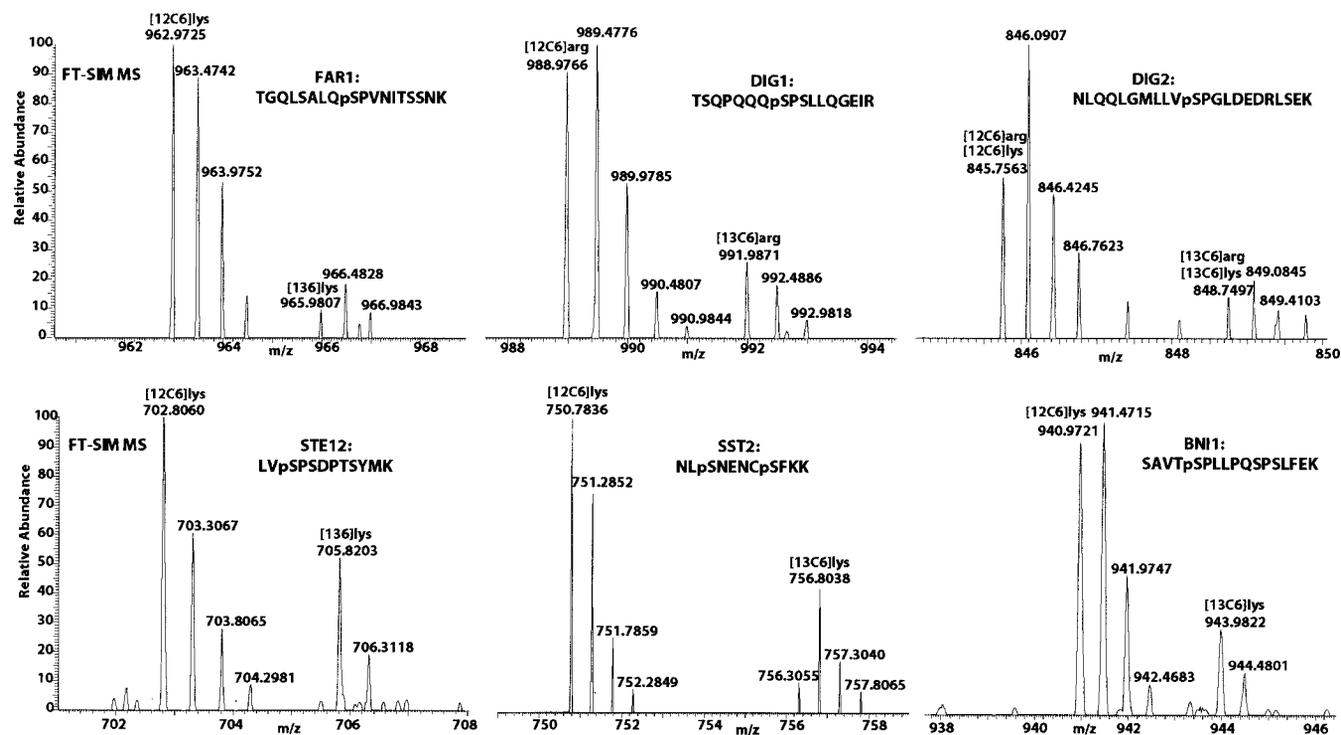
FIG. 7. **Quantitation of Fus3p substrate phosphorylation sites from phosphopeptide SILAC doublets.** The panels show FTICR-SIM MS spectra from different identified phosphopeptide pairs of known Fus3p substrates: Far1, Dig1, Dig2, Ste12, SstII, and Bni1. The lower mass isotope clusters represent the α-factor-stimulated and normal arginine- and lysine-encoded cell population, whereas the higher isotope clusters derive from the heavy isotope-labeled ([$^{13}C_6$]arginine and [$^{13}C_6$]lysine) control state. All displayed Fus3p substrates exhibit specific activation by phosphorylation upon α-factor treatment.

peptides with phosphorylation at either threonine 180 or tyrosine 182 were identified; both were highly induced by pheromone treatment (Fig. 6). The doubly phosphorylated peptide was not found probably due to limitations of our method in its current implementation, which might favor the detection of singly phosphorylated peptides.

The carboxyl-terminal cytoplasmic portion of Ste2p becomes hyperphosphorylated in response to α-factor and has been implicated in the modulation of Ste2p activity and its endocytosis (70), but the role of Ste2p phosphorylation is not yet completely understood. Recently it was found that exchange of the four most distal serines and threonines (from serine 398 to threonine 425) to alanines increased the sensitivity of Ste2p for α-factor (71) and that phosphorylation of the carboxyl-terminal domain is important for receptor endocytosis (72). We identified two phosphorylation sites on serine 366 and threonine 382 of which serine 366 is up-regulated moderately (1.4-fold) and threonine 382 is up-regulated strongly (4.7-fold) by α-factor. These two phosphorylation sites lie between the sequence SINNDAKSS required for phosphorylation-regulated ubiquitination and subsequent endocytosis and the four most distal sites found to modulate receptor sensitivity. The biological role of these phosphorylation events therefore needs further genetic analysis.

Ste20p is autophosphorylated and is a substrate for phos-

phorylation by Cdc28p-Cln2p. At least 13 different phosphorylation sites have been identified by mass spectrometry (24). We found phosphorylation at serine 169, serine 418, and serine 585 of which phosphoserine 418 is strongly induced by α-factor. None of these sites was found to be phosphorylated by Cdc28p-Cln2p (24).

Several substrates for phosphorylation by the MAP kinase Fus3p have been reported in the literature, including Far1p, Dig1p, Dig2p, Ste12p, Sst2p, and Bni1p. Pheromone-induced phosphorylation sites were identified for all of those proteins (Fig. 7 and Table III). With the exception of Sst2p, all phosphorylation occurred on proline-directed serines. The phosphorylation sites found in Sst2p do not correspond to the previously identified Fus3p phosphorylation site at serine 539 (64) and might therefore be caused by other kinases. In this case, the increase in phosphorylation could reflect the transcriptional activation of *SST2* in response to α-factor. Prediction of the identified phosphorylation sites by NetPhos (73) yielded values above threshold only for Ste12p and Sst2p, suggesting that Fus3p recognizes a so far uncharacterized sequence motif (Table III).

Dig1p and Dig2p interact with both the MAP kinase Fus3p and Ste12p, and this complex formation is thought to inhibit the transcriptional activation of genes with pheromone-responsive elements by Ste12p (48). Phosphorylation of Dig1p

TABLE III
Identified phosphorylation sites of known Fus3 targets

Protein name	Phosphorylation site	NetPhos score	Up-regulation
			-fold
Ste12p	EKLVpSPSDP	0.998	4.5
Far1p	SALQpSPVNI	0.198	8.3
Dig1p	PQQQpSPSLL	0.021	3.8
Dig2p	MLLVpSPGLD	0.447	6.6
Bni1p	SAVTpSPLLP	0.025	1.8
Sst2p	APNGpSTIDL	0.993	3.4
Sst2p	SKNLpSNENCpSFKK	0.901/0.579	5.5

and Dig2p by activated Fus3p leads to the release of Ste12p and subsequent transcriptional activation, but the phosphorylation sites for Dig1p p have not yet been mapped. We found Dig1p and Dig2p peptides with phosphorylation at serine 395 and serine 34, respectively, that were up-regulated 3.8- and 6-fold (Table III). These novel phosphorylation sites could serve as starting points for the elucidation of the regulatory mechanism by which Fus3p modulates Dig1p and Dig2p activity.

Conclusion and Perspectives—In this study, we combined a number of technologies to determine quantitative changes in the phosphoproteome. We encoded yeast proteomes with stable isotopes using SILAC to enable relative quantitation of all peptides and used SCX and IMAC to enrich phosphopeptides. MS^3 on a hybrid linear ion trap Fourier transform mass spectrometer provided a highly sensitive and confident detection method for phosphopeptides.

This study demonstrates that quantitative phosphoproteomics can be used to characterize the activation of a signaling pathway all the way from receptor through MAP kinases to transcription factors. As a model, we used the yeast pheromone signaling pathway, a prototype MAP kinase pathway. Peptides phosphorylated in response to stimulus span the whole range of pheromone response, including receptor activation, kinase cascade, cytoskeletal remodeling, and other downstream processes.

There exist several different signaling pathways in yeast that partly rely on the same components of the signaling cascade. Further experiments could therefore be designed to analyze the phosphoproteome in response to other signals such as high osmolarity, starvation, or other stress factors. Such analyses could be used to examine the differences and the cross-talk between these signaling pathways and to gain a better understanding of how they are regulated. Large scale quantitative phosphoproteomic data sets like the one presented here can also be used to improve adaptive computational methods for prediction of protein phosphorylation sites and to refine mathematical models for cell signaling networks.

Another obvious follow-up to this study could include recording the effects on the phosphoproteomes of mutant yeast strains deficient in each component of the pheromone signaling pathway. We note that for such perturbation experiments the depth of analysis achieved in this report is probably already sufficient since all major signaling branches are covered. Timing of the signaling events and downstream processes could be resolved by analyzing samples from cells incubated for different periods with pheromone using SILAC triple encoding as we have already demonstrated in the epidermal growth factor signaling pathway (30).

For this study, 14 different fractions with enriched phosphopeptides were analyzed by LC-MS/MS from the same sample. The result was the identification of more than 700 phosphopeptides of which 139 were differentially regulated at least 2-fold, and at least 20 belonged to proteins with explicit functions in pheromone signaling and mating. However, even using affinity enrichment strategies and high sensitivity mass spectrometry, phosphopeptide coverage was not comprehensive. Not all known phosphopeptides in the pheromone response pathway are represented in our data set. This is most likely due to a combination of factors including inefficiencies in protein extraction and enzymatic digestion and the uneven sampling of peptides for fragmentation in current LC-MS/MS methods. While we have shown that phosphorylation sites could be determined from extremely low level phosphoproteins, other phosphopeptides may have very low level stoichiometry combined with unfavorable ionization characteristics and require even greater analytical sensitivity. We envision, however, that further improvements in sample preparation and mass spectrometry will increase the phosphopeptide coverage and reduce the number of cells and chromatographic fractions needed for an analysis. Regardless of these factors, the present depth of phosphoproteome analysis was sufficient to demonstrate the activation of the entire pheromone response pathway. Furthermore if a pathway has been characterized in depth, specific marker phosphopeptides can then serve as indicators for the activation of that signaling pathway.

Signaling in yeast is prototypic for eukaryotic cells, and our methods should therefore be applicable to mammalian cells. Despite the considerably higher complexity in the human organism, signaling pathways could be characterized in the same way as done here for yeast. The definition of marker phosphopeptides would allow testing samples in a reason-

ably fast way for active pathways. Applications of this method could be the analysis of cancer cells or the study of the effects of drugs targeting GPCRs and kinases on cellular phosphorylation.

REFERENCES

1. Mann, M., and Jensen, O. N. (2003) Proteomic analysis of post-translational modifications. *Nat. Biotechnol.* **21,** 255–261
2. Jensen, O. N. (2004) Modification-specific proteomics: characterization of post-translational modifications by mass spectrometry. *Curr. Opin. Chem. Biol.* **8,** 33–41
3. Hunter, T. (2000) Signaling—2000 and beyond. *Cell* **100,** 113–127
4. Cohen, P. (2002) Protein kinases—the major drug targets of the twenty-first century? *Nat. Rev. Drug Discov.* **1,** 309–315
5. Mann, M., Ong, S. E., Grønborg, M., Steen, H., Jensen, O. N., and Pandey, A. (2002) Analysis of protein phosphorylation using mass spectrometry: deciphering the phosphoproteome. *Trends Biotechnol.* **20,** 261–268
6. Posewitz, M. C., and Tempst, P. (1999) Immobilized gallium(III) affinity chromatography of phosphopeptides. *Anal. Chem.* **71,** 2883–2892
7. Nuhse, T. S., Stensballe, A., Jensen, O. N., and Peck, S. C. (2003) Large-scale analysis of in vivo phosphorylated membrane proteins by immobilized metal ion affinity chromatography and mass spectrometry. *Mol. Cell. Proteomics* **2,** 1234–1243
8. Brill, L. M., Salomon, A. R., Ficarro, S. B., Mukherji, M., Stettler-Gill, M., and Peters, E. C. (2004) Robust phosphoproteomic profiling of tyrosine phosphorylation sites from human T cells using immobilized metal affinity chromatography and tandem mass spectrometry. *Anal. Chem.* **76,** 2763–2772
9. Ficarro, S. B., McCleland, M. L., Stukenberg, P. T., Burke, D. J., Ross, M. M., Shabanowitz, J., Hunt, D. F., and White, F. M. (2002) Phosphoproteome analysis by mass spectrometry and its application to *Saccharomyces cerevisiae*. *Nat. Biotechnol.* **20,** 301–305
10. Stensballe, A., and Jensen, O. N. (2004) Phosphoric acid enhances the performance of Fe(III) affinity chromatography and matrix-assisted laser desorption/ionization tandem mass spectrometry for recovery, detection and sequencing of phosphopeptides. *Rapid Commun. Mass Spectrom.* **18,** 1721–1730
11. Stensballe, A., Andersen, S., and Jensen, O. N. (2001) Characterization of phosphoproteins from electrophoretic gels by nanoscale Fe(III) affinity chromatography with off-line mass spectrometry analysis. *Proteomics* **1,** 207–222
12. Collins, M. O., Yu, L., Coba, M. P., Husi, H., Campuzano, I., Blackstock, W. P., Choudhary, J. S., and Grant, S. G. (2005) Proteomic analysis of *in vivo* phosphorylated synaptic proteins. *J. Biol. Chem.* **280,** 5972–5982
13. Aebersold, R., and Mann, M. (2003) Mass spectrometry-based proteomics. *Nature* **422,** 198–207
14. Steen, H., and Mann, M. (2004) The abc's (and xyz's) of peptide sequencing. *Nat. Rev. Mol. Cell. Biol.* **5,** 699–711
15. McLuckey, S. A. (1992) Principles of collisional activation in analytical mass spectrometry. *J. Am. Soc. Mass Spectrom.* **3,** 599–614
16. Stensballe, A., Jensen, O. N., Olsen, J. V., Haselmann, K. F., and Zubarev, R. A. (2000) Electron capture dissociation of singly and multiply phosphorylated peptides. *Rapid Commun. Mass Spectrom.* **14,** 1793–1800
17. Shi, S. D., Hemling, M. E., Carr, S. A., Horn, D. M., Lindh, I., and McLafferty, F. W. (2001) Phosphopeptide/phosphoprotein mapping by electron capture dissociation mass spectrometry. *Anal. Chem.* **73,** 19–22
18. Syka, J. E., Coon, J. J., Schroeder, M. J., Shabanowitz, J., and Hunt, D. F. (2004) Peptide and protein sequence analysis by electron transfer dissociation mass spectrometry. *Proc. Natl. Acad. Sci. U. S. A.* **101,** 9528–9533
19. Beausoleil, S. A., Jedrychowski, M., Schwartz, D., Elias, J. E., Villen, J., Li, J., Cohn, M. A., Cantley, L. C., and Gygi, S. P. (2004) Large-scale characterization of HeLa cell nuclear phosphoproteins. *Proc. Natl. Acad. Sci. U. S. A.* **101,** 12130–12135
20. Olsen, J. V., and Mann, M. (2004) Improved peptide identification in proteomics by two consecutive stages of mass spectrometric fragmentation. *Proc. Natl. Acad. Sci. U. S. A.* **101,** 13417–13422
21. Syka, J. E., Marto, J. A., Bai, D. L., Horning, S., Senko, M. W., Schwartz, J. C., Ueberheide, B., Garcia, B., Busby, S., Muratore, T., Shabanowitz, J., and Hunt, D. F. (2004) Novel linear quadrupole ion trap/FT mass spectrometer: performance characterization and use in the comparative analysis of histone H3 post-translational modifications. *J. Proteome Res.* **3,** 621–626
22. Nuhse, T. S., Stensballe, A., Jensen, O. N., and Peck, S. C. (2004) Phosphoproteomics of the Arabidopsis plasma membrane and a new phosphorylation site database. *Plant Cell* **16,** 2394–2405
23. Oda, Y., Huang, K., Cross, F. R., Cowburn, D., and Chait, B. T. (1999) Accurate quantitation of protein expression and site-specific phosphorylation. *Proc. Natl. Acad. Sci. U. S. A.* **96,** 6591–6596
24. Ibarrola, N., Kalume, D. E., Gronborg, M., Iwahori, A., and Pandey, A. (2003) A proteomic approach for quantitation of phosphorylation using stable isotope labeling in cell culture. *Anal. Chem.* **75,** 6043–6049
25. Stover, D. R., Caldwell, J., Marto, J., Root, R., Mestan, J., Stumm, M., Ornatsky, O., Orsi, C., Radosevic, N., Liao, L., Fabbro, D., and Moran, M. F. (2004) Differential phosphoprofiles of EGF and EGFR kinase inhibitor-treated human tumor cells and mouse xenografts. *Clin. Proteomics* **1,** 069–080
26. Ong, S. E., Blagoev, B., Kratchmarova, I., Kristensen, D. B., Steen, H., Pandey, A., and Mann, M. (2002) Stable isotope labeling by amino acids in cell culture, SILAC, as a simple and accurate approach to expression proteomics. *Mol. Cell. Proteomics* **1,** 376–386
27. Ong, S. E., Kratchmarova, I., and Mann, M. (2003) Properties of ^{13}C-substituted arginine in stable isotope labeling by amino acids in cell culture (SILAC). *J. Proteome Res.* **2,** 173–181
28. Zhu, H., Pan, S., Gu, S., Bradbury, E. M., and Chen, X. (2002) Amino acid residue specific stable isotope labeling for quantitative proteomics. *Rapid Commun. Mass Spectrom.* **16,** 2115–2123
29. Schulze, W. X., and Mann, M. (2004) A novel proteomic screen for peptide-protein interactions. *J. Biol. Chem.* **279,** 10756–10764
30. Blagoev, B., Ong, S. E., Kratchmarova, I., and Mann, M. (2004) Temporal analysis of phosphotyrosine-dependent signaling networks by quantitative proteomics. *Nat. Biotechnol.* **22,** 1139–1145
31. Blagoev, B., Kratchmarova, I., Ong, S. E., Nielsen, M., Foster, L. J., and Mann, M. (2003) A proteomics strategy to elucidate functional protein-protein interactions applied to EGF signaling. *Nat. Biotechnol.* **21,** 315–318
32. Wang, Y., and Dohlman, H. G. (2004) Pheromone signaling mechanisms in yeast: a prototypical sex machine. *Science* **306,** 1508–1509
33. Dohlman, H. G. (2002) G proteins and pheromone signaling. *Annu. Rev. Physiol.* **64,** 129–152
34. Bardwell, L. (2004) A walk-through of the yeast mating pheromone response pathway. *Peptides* **25,** 1465–1476
35. Rappsilber, J., Ishihama, Y., and Mann, M. (2003) Stop and go extraction tips for matrix-assisted laser desorption/ionization, nanoelectrospray, and LC/MS sample pretreatment in proteomics. *Anal. Chem.* **75,** 663–670
36. Olsen, J. V., Ong, S. E., and Mann, M. (2004) Trypsin cleaves exclusively C-terminal to arginine and lysine residues. *Mol. Cell. Proteomics* **3,** 608–614

37. Elortza, F., Nuhse, T. S., Foster, L. J., Stensballe, A., Peck, S. C., and Jensen, O. N. (2003) Proteomic analysis of glycosylphosphatidylinositol-anchored membrane proteins. *Mol. Cell. Proteomics* **2,** 1261–1270

38. Hinsby, A. M., Olsen, J. V., and Mann, M. (2004) Tyrosine phosphoproteomics of fibroblast growth factor signaling: a role for insulin receptor substrate-4. *J. Biol. Chem.* **279,** 46438–46447

39. Andersen, J. S., Wilkinson, C. J., Mayor, T., Mortensen, P., Nigg, E. A., and Mann, M. (2003) Proteomic characterization of the human centrosome by protein correlation profiling. *Nature* **426,** 570–574

40. Annan, R. S., and Carr, S. A. (1996) Phosphopeptide analysis by matrix-assisted laser desorption time-of-flight mass spectrometry. *Anal. Chem.* **68,** 3413–3421

41. Roberts, C. J., Nelson, B., Marton, M. J., Stoughton, R., Meyer, M. R., Bennett, H. A., He, Y. D., Dai, H., Walker, W. L., Hughes, T. R., Tyers, M., Boone, C., and Friend, S. H. (2000) Signaling and circuitry of multiple MAPK pathways revealed by a matrix of global gene expression profiles. *Science* **287,** 873–880

42. Lew, D. J., and Kornbluth, S. (1996) Regulatory roles of cyclin dependent kinase phosphorylation in cell cycle control. *Curr. Opin. Cell Biol.* **8,** 795–804

43. Leeuw, T., Wu, C., Schrag, J. D., Whiteway, M., Thomas, D. Y., and Leberer, E. (1998) Interaction of a G-protein β-subunit with a conserved sequence in Ste20/PAK family protein kinases. *Nature* **391,** 191–195

44. Lamson, R. E., Winters, M. J., and Pryciak, P. M. (2002) Cdc42 regulation of kinase activity and signaling by the yeast p21-activated kinase Ste20. *Mol. Cell. Biol.* **22,** 2939–2951

45. Inouye, C., Dhillon, N., and Thorner, J. (1997) Ste5 RING-H2 domain: role in Ste4-promoted oligomerization for yeast pheromone signaling. *Science* **278,** 103–106

46. Elion, E. A., Satterberg, B., and Kranz, J. E. (1993) FUS3 phosphorylates multiple components of the mating signal transduction cascade: evidence for STE12 and FAR1. *Mol. Biol. Cell* **4,** 495–510

47. Olson, K. A., Nelson, C., Tai, G., Hung, W., Yong, C., Astell, C., and Sadowski, I. (2000) Two regulators of Ste12p inhibit pheromone-responsive transcription by separate mechanisms. *Mol. Cell. Biol.* **20,** 4199–4209

48. Tedford, K., Kim, S., Sa, D., Stevens, K., and Tyers, M. (1997) Regulation of the mating pheromone and invasive growth responses in yeast by two MAP kinase substrates. *Curr. Biol.* **7,** 228–238

49. Horecka, J., and Sprague, G. F., Jr. (1996) Identification and characterization of FAR3, a gene required for pheromone-mediated G1 arrest in *Saccharomyces cerevisiae. Genetics* **144,** 905–921

50. Kemp, H. A., and Sprague, G. F., Jr. (2003) Far3 and five interacting proteins prevent premature recovery from pheromone arrest in the budding yeast *Saccharomyces cerevisiae. Mol. Cell. Biol.* **23,** 1750–1763

51. Chang, F., and Herskowitz, I. (1990) Identification of a gene necessary for cell cycle arrest by a negative growth factor of yeast: FAR1 is an inhibitor of a G1 cyclin, CLN2. *Cell* **63,** 999–1011

52. Peter, M., and Herskowitz, I. (1994) Direct inhibition of the yeast cyclin-dependent kinase Cdc28-Cln by Far1. *Science* **265,** 1228–1231

53. Tyers, M., and Futcher, B. (1993) Far1 and Fus3 link the mating pheromone signal transduction pathway to three G1-phase Cdc28 kinase complexes. *Mol. Cell. Biol.* **13,** 5659–5669; Correction (1994) *Mol. Cell. Biol.* **14,** 2222

54. Gartner, A., Jeoung, D.-I., Bourlat, S., Cross, F. R., and Ammerer, G. (1998) Pheromone-dependent G1 cell cycle arrest requires Far1 phosphorylation, but may not involve inhibition of Cdc28-Cln2 kinase, *in vivo. Mol. Cell. Biol.* **18,** 3681–3691

55. Pruyne, D., and Bretscher, A. (2000) Polarization of cell growth in yeast. I. Establishment and maintenance of polarity states. *J. Cell Sci.* **113,** 365–375

56. Pruyne, D., and Bretscher, A. (2000) Polarization of cell growth in yeast. *J. Cell Sci.* **113,** 571–585

57. White, J. M., and Rose, M. D. (2001) Yeast mating: getting close to membrane merger. *Curr. Biol.* **11,** R16–R20

58. Evangelista, M., Blundell, K., Longtine, M. S., Chow, C. J., Adames, N., Pringle, J. R., Peter, M., and Boone, C. (1997) Bni1p, a yeast formin linking Cdc42p and the actin cytoskeleton during polarized morphogenesis. *Science* **276,** 118–122

59. Gourlay, C. W., Dewar, H., Warren, D. T., Costa, R., Satish, N., and Ayscough, K. R. (2003) An interaction between Sla1p and Sla2p plays a role in regulating actin dynamics and endocytosis in budding yeast. *J. Cell Sci.* **116,** 2551–2564

60. Shih, S. C., Katzmann, D. J., Schnell, J. D., Sutanto, M., Emr, S. D., and Hicke, L. (2002) Epsins and Vps27p/Hrs contain ubiquitin-binding domains that function in receptor endocytosis. *Nat. Cell Biol.* **4,** 389–393

61. Madden, K., and Snyder, M. (1998) Cell polarity and morphogenesis in budding yeast. *Annu. Rev. Microbiol.* **52,** 687–744

62. Apanovitch, D. M., Slep, K. C., Sigler, P. B., and Dohlman, H. G. (1998) Sst2 is a GTPase-activating protein for Gpa1: purification and characterization of a cognate RGS-Gα protein pair in yeast. *Biochemistry* **37,** 4815–4822

63. Dohlman, H. G., Song, J., Ma, D., Courchesne, W. E., and Thorner, J. (1996) Sst2, a negative regulator of pheromone signaling in the yeast *Saccharomyces cerevisiae*: expression, localization, and genetic interaction and physical association with Gpa1 (the G-protein α subunit). *Mol. Cell. Biol.* **16,** 5194–5209

64. Garrison, T. R., Zhang, Y., Pausch, M., Apanovitch, D., Aebersold, R., and Dohlman, H. G. (1999) Feedback phosphorylation of an RGS protein by MAP kinase in yeast. *J. Biol. Chem.* **274,** 36387–36391

65. Lee, S. E., Frenz, L. M., Wells, N. J., Johnson, A. L., and Johnston, L. H. (2001) Order of function of the budding-yeast mitotic exit-network proteins Tem1, Cdc15, Mob1, Dbf2, and Cdc5. *Curr. Biol.* **11,** 784–788

66. de Bruin, R. A., McDonald, W. H., Kalashnikova, T. I., Yates, J., III, and Wittenberg, C. (2004) Cln3 activates G1-specific transcription via phosphorylation of the SBF bound repressor Whi5. *Cell* **117,** 887–898

67. Munchow, S., Sauter, C., and Jansen, R. (1999) Association of the class V myosin Myo4p with a localised messenger RNA in budding yeast depends on She proteins. *J. Cell Sci.* **112,** 1511–1518

68. Ghaemmaghami, S., Huh, W. K., Bower, K., Howson, R. W., Belle, A., Dephoure, N., O'Shea, E. K., and Weissman, J. S. (2003) Global analysis of protein expression in yeast. *Nature* **425,** 737–741

69. Gartner, A., Nasmyth, K., and Ammerer, G. (1992) Signal transduction in *Saccharomyces cerevisiae* requires tyrosine and threonine phosphorylation of FUS3 and KSS1. *Genes Dev.* **6,** 1280–1292

70. Reneke, J. E., Blumer, K. J., Courchesne, W. E., and Thorner, J. (1988) The carboxy-terminal segment of the yeast α-factor receptor is a regulatory domain. *Cell* **55,** 221–234

71. Chen, Q., and Konopka, J. B. (1996) Regulation of the G-protein-coupled α-factor pheromone receptor by phosphorylation. *Mol. Cell. Biol.* **16,** 247–257

72. Hicke, L., Zanolari, B., and Riezman, H. (1998) Cytoplasmic tail phosphorylation of the α-factor receptor is required for its ubiquitination and internalization. *J. Cell Biol.* **141,** 349–358

73. Blom, N., Gammeltoft, S., and Brunak, S. (1999) Sequence and structure-based prediction of eukaryotic protein phosphorylation sites. *J. Mol. Biol.* **294,** 1351–1362